ACIBADEM MEHMET ALİ AYDINLAR UNIVERSITY
GRADUATE SCHOOL OF NATURAL AND APPLIED SCIENCES

INVESTIGATION OF THE EFFECT OF FOLATE RECEPTOR-TARGETED AND 3-ABA-LOADED POLYMERIC MICELLES AND THEIR IN VITRO EVALUATIONS

İPEK DUYGU TÜRKDEMİR

M.Sc. THESIS

DEPARTMENT OF BIOMATERIALS

SUPERVISOR

Assoc. Prof. Özgül Gök Özatay

ISTANBUL-2025

ACIBADEM MEHMET ALİ AYDINLAR UNIVERSITY
GRADUATE SCHOOL OF NATURAL AND APPLIED SCIENCES

INVESTIGATION OF THE EFFECT OF FOLATE RECEPTOR-TARGETED AND 3-ABA-LOADED POLYMERIC MICELLES AND THEIR IN VITRO EVALUATIONS

İPEK DUYGU TÜRKDEMİR

M.Sc. THESIS

DEPARTMENT OF BIOMATERIALS

SUPERVISOR

Assoc. Prof. Özgül Gök Özatay

ISTANBUL-2025

DECLARATION

I declare that this thesis work is my own. I engaged in no unethical behaviour at any stage from the planning to the writing of the thesis. I obtained all the information in this thesis in accordance with academic and ethical rules. I cited all the information and comments that were not received with this thesis work, and I provided resources in the list of references. I also declare that there was no violation of any patents or copyrights during the study and writing of this thesis.

06/01/2026

İpek Duygu Türkdemir

PREFACE AND ACKNOWLEDGEMENT

Firstly, I would like to express my sincere gratitude to my thesis advisor, Associate Prof. Dr. Özgül Gök Özatay for her unwavering support throughout this entire process, her patience, and her invaluable contributions to my academic development. I am incredibly fortunate to have had her as a mentor and guide since 2019, when I was just an undergraduate.

I am also profoundly grateful to all former and current members of the GÖK Research Group, whose support and camaraderie have made my master's journey both enriching and enjoyable (13). A special thank you to Aleyna Sezgin, Kübra Üstüner, Berna Sayın, Tuğba Menteş, and Berivan Kakız for always being my second family. I am equally thankful to have met Zeynep Poyraz, Selin Yazıcı, Tuğçe Yüksel, İdil Özdemir, and Elis Çetin along this journey. Moreover, I would like to extend my heartfelt appreciation to Aslıhan Akalınlı and Büşra Yaşlı for their unwavering support and assistance throughout my two years as a master's student. I am fortunate to have such wonderful friends, and I cherish them.

I would also like to express my deepest gratitude to my parents, Pervin Türkdemir and Mehmet Haluk Türkdemir, my sister-in-law, Pınar Türkdemir, and my nephew, Karan Türkdemir, for their unwavering support and unconditional love.

LIST OF ABBREVIATIONS AND SYMBOLS

3-AB	3-Aminobenzamide
BER	Base Excision Repair
CCK-8	Cell Counting Kit-8
DAPI	4′,6-Diamidino-2-phenylindole
DLS	Dynamic Light Scattering
DMEM	Dulbecco's Modified Eagle Medium
DMSO	Dimethyl Sulfoxide
EDC	N-(3-Dimethylaminopropyl)-N′-ethylcarbodiimide
EPR	Enhanced Permeability and Retention
FA	Folic Acid
FDA	Food and Drug Administration
HR	Homologous Recombination
LC/MS-MS	Liquid Chromatography Tandem Mass Spectrometry
MPS	Mononuclear Phagocyte System
NAD+	Nicotinamide Adenine Dinucleotide
NP	Nanoparticle
PARP	Poly (ADP-ribose) Polymerase
PBS	Phosphate-Buffered Saline
PCL	Polycaprolactone
PEG	Polyethylene Glycol
PEG–PLGA	Polyethylene Glycol–Poly(lactic-co-glycolic acid)
PLA	Polylactic Acid
PLGA	Poly(lactic-co-glycolic acid)
ROS	Reactive Oxygen Species
SEM	Scanning Electron Microscopy
TEA	Triethylamine

THF	Tetrahydrofuran
ZP	Zeta Potential

TABLE OF CONTENTS

LIST OF FIGURES

LIST OF TABLES

ÖZET

Bu tez çalışmasında, klasik bir PARP-1 inhibitörü olan 3-aminobenzamidin (3-AB), folat reseptörüne hedefli PEG–PLGA mikellerine enkapsüle edilerek over kanseri tedavisindeki terapötik potansiyeli araştırılmıştır. Biyouyumlu yapıları, kontrollü salım özellikleri ve tümör hedefleme kapasiteleriyle bilinen polimerik mikeller, 3-AB'nin farmakokinetik kısıtlarını aşmak ve sitotoksik etkisini artırmak amacıyla kullanılmıştır. İn vitro model olarak, yüksek düzeyde folat reseptörü ekspresyonuna sahip SKOV-3 over kanseri hücre hattı tercih edilmiştir.

Elde edilen veriler, folik asit ile fonksiyonelleştirilen mikellerin, serbest 3-AB ve hedeflenmemiş mikellere kıyasla hücre içine alımı ve sitotoksisitesini belirgin şekilde artırdığını göstermiştir. Bu artışın, reseptör aracılı endositoz ile sağlandığı düşünülmektedir. Ayrıca, hedeflenmemiş PEG–PLGA miseller de EPR (enhanced permeability and retention) etkisinden faydalanarak serbest ilaca göre daha yüksek etkinlik göstermiştir. PEG modifikasyonunun, dolaşım süresini uzatma ve immün sistem tarafından tanınmayı azaltma gibi katkıları da çalışmada gözlenmiştir.

Sonuç olarak, bu tez çalışması, 3-AB'nin PEG–PLGA mikellerle özellikle folik asit aracılığıyla hedefli olarak taşınmasının, over kanseri tedavisinde umut vaat eden bir strateji olabileceğini ortaya koymuştur. Bu bulgular, nanoformülasyonlu PARP inhibitörlerinin kişiselleştirilmiş kanser tedavisindeki potansiyelini desteklemektedir.

Anahtar Kelimeler: Over Kanseri, PARP İnhibitörleri, 3-Aminobenzamid, PEG-PLGA, Polimerik Mikeller

ABSTRACT

This thesis investigates the therapeutic potential of folate receptor-targeted PEG–PLGA micelles encapsulating 3-aminobenzamide (3-AB), a classical PARP-1 inhibitor, in the treatment of ovarian cancer. Polymeric micelles, known for their biocompatibility, controlled release capability, and tumor-targeting potential, were employed to overcome the pharmacokinetic limitations of 3-AB and enhance its cytotoxicity. SKOV-3 ovarian cancer cells, which overexpress folate receptors, were selected as the *in vitro* model.

The results demonstrated that FA-functionalized micelles significantly improved cellular uptake and cytotoxicity of 3-AB compared to free drug and non-targeted micelles, likely through receptor-mediated endocytosis. Non-targeted PEG–PLGA micelles also showed improved efficacy, likely benefiting from the enhanced permeability and retention (EPR) effect. The study highlights the added advantage of PEGylation in prolonging systemic circulation and minimizing immune recognition. While the findings are promising, further studies involving additional ovarian cancer models, in vivo validation, and combinatorial therapeutic strategies are needed. Nonetheless, this work provides a foundation for the potential use of nanoformulated 3-AB in targeted ovarian cancer therapy and reinforces the utility of ligand-conjugated micelles in improving drug delivery outcomes.

Keywords: Ovarian Cancer, PARP Inhibitors, 3-Aminobenzamide, PEG-PLGA, Polymeric Micelles

1. INTRODUCTION AND AIM

1.1. Introduction

Cancer remains one of the leading causes of morbidity and mortality worldwide, posing a major global health challenge. Conventional chemotherapeutic approaches, while often effective in reducing tumour burden, suffer from significant limitations, including poor solubility of certain drugs, systemic toxicity, and a lack of selectivity towards cancer cells. These drawbacks can lead to severe side effects and reduced patient compliance, highlighting the need for more precise and efficient drug delivery strategies.

Nanomedicine has emerged as a transformative approach to overcome these challenges by utilising nanoscale carriers for targeted drug delivery. Polymeric micelles, in particular, have gained attention due to their ability to encapsulate hydrophobic drugs within their core while maintaining stability and biocompatibility in physiological environments. They are formed through the self-assembly of amphiphilic block copolymers, where the hydrophobic segment forms the inner core that entraps the drug, and the hydrophilic segment forms an outer shell that prolongs systemic circulation.

Poly(ethylene glycol)–poly(lactic-co-glycolic acid) (PEG–PLGA) copolymers are among the most widely studied materials for micelle formation, owing to their biodegradability, tunable physicochemical properties, and regulatory approval for medical use. In addition to passive targeting via the enhanced permeability and retention (EPR) effect, the therapeutic potential of micelles can be further enhanced through active targeting strategies. One such approach is functionalisation with folic acid (FA), which has a high affinity for folate receptors that are overexpressed on the surface of various cancer cells but minimally expressed in most healthy tissues. This targeting mechanism can facilitate receptor-mediated endocytosis, thereby increasing the intracellular concentration of the therapeutic agent.

Poly(ADP-ribose) polymerase (PARP) is a key enzyme in DNA repair pathways, particularly in base excision repair (BER). Inhibiting PARP activity can

enhance the cytotoxic effects of DNA damage, especially in cancer cells with pre-existing defects in DNA repair mechanisms, such as BRCA mutations. 3-Aminobenzamide (3-AB) is a well-known PARP inhibitor that can disrupt cancer cell survival, but its clinical application is limited by poor water solubility and non-specific distribution. Encapsulating 3-AB within FA-targeted PEG–PLGA micelles offers a potential means to enhance solubility, improve tumour-specific delivery, and reduce systemic toxicity.

1.2 Aim

The primary objective of this study is to develop and evaluate folate receptor-targeted, 3-aminobenzamide-loaded PEG–PLGA micelles for the inhibition of cancer-associated PARP protein. The specific aims are to:

1. Synthesise and optimise FA-PEG-PLGA micelles and non-targeted PEG–PLGA micelles using a solvent evaporation technique.
2. Characterise the micelles in terms of hydrodynamic diameter, polydispersity index (PDI), surface charge, drug encapsulation efficiency, and in vitro drug release profile under physiological and acidic conditions.
3. Compare the cytotoxicity profiles of targeted and non-targeted micelles with free 3-AB in relevant cancer cell lines and a control fibroblast cell line.
4. Assess cellular uptake efficiency of targeted versus non-targeted micelles, with a focus on the role of folate-mediated active targeting.

2. BACKGROUND

2.1 DRUG DELIVERY SYSTEMS

The National Cancer Institute defines a drug as any substance—excluding food—that is used to prevent, diagnose, treat, or alleviate symptoms of diseases or abnormal conditions (1). Although essential for therapeutic purposes, drugs often fail to function optimally when administered alone. The method of administration can significantly influence their metabolic fate and biodistribution (1–3). Drug delivery systems aim to ensure that therapeutic agents reach diseased cells at appropriate concentrations, which is particularly promising in cancer therapy where precise targeting is crucial (4–6).

A drug delivery system facilitates the introduction of an active pharmaceutical ingredient (API) to achieve the desired therapeutic outcome while minimizing adverse effects (1,7). Traditional delivery forms such as tablets, capsules, or powders face several limitations, including severe side effects, poor specificity, and multidrug resistance (1,8). Accordingly, drug delivery strategies are generally categorized into three main approaches: (i) optimizing the route of administration and absorption, (ii) controlling the release profile, and (iii) directing the therapeutic agent to the specific site of action (1,9).

Drug delivery systems have gained significant importance due to advancements in biomaterials, enabling more effective therapeutic strategies (10). The development of nanoparticles and polymers has revolutionized targeted drug delivery by enhancing specificity and reducing systemic side effects. Targeted drug delivery represents an advanced approach designed to selectively transport drugs to desired sites, thereby minimizing drug accumulation in non-target tissues (3,4). This strategy is applicable across various diseases, including cancer and diabetes, where precision in drug localization is critical. Drug targeting is generally categorized into two subgroups: passive and active targeting.

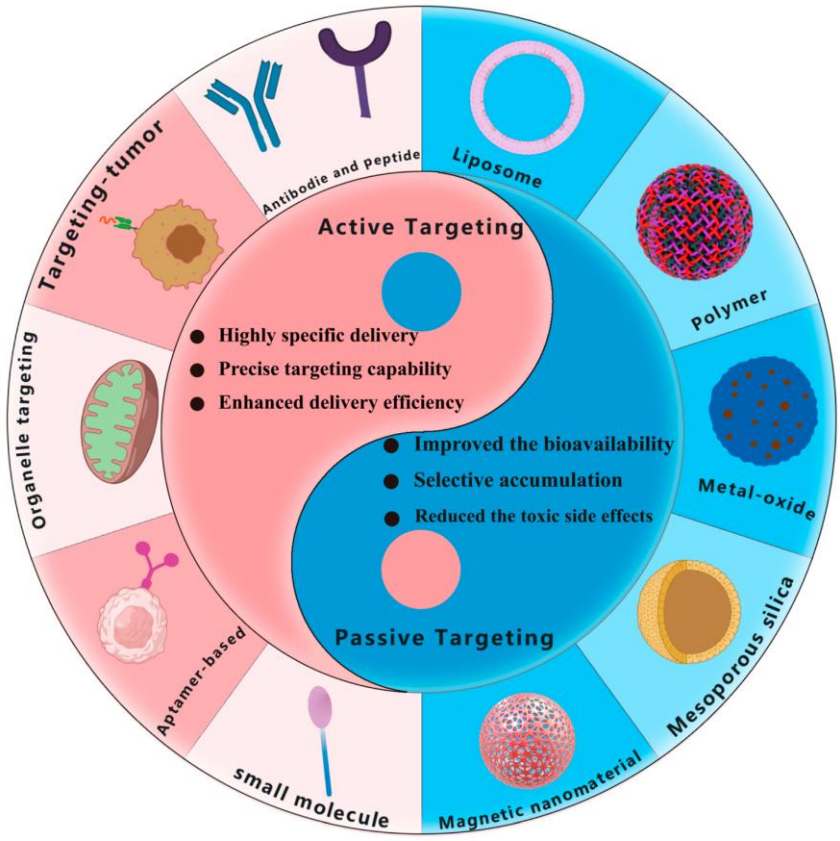

Figure 2.1. Passive and Active Targeting in Drug Delivery

2.1.1 Passive Targeting

The passive targeting mechanism employs nanocarriers to deliver drugs directly to cells or tumor mesenchyme via capillary pores with convection or diffusion (15). In tumor mesenchyme, where convection is limited and interstitial pressure is high, diffusion primarily serves as the method for drug transport (18). The Enhanced Permeation and Retention (EPR) effect indicates that tumours possess capillaries that facilitate the penetration of nanocarriers into these areas, forming the basis of the passive targeting strategy to guide nanocarriers toward solid tumours (19). Examples of drug delivery systems utilising passive targeting include polymeric nanoparticles, liposomes, and metal oxide nanoparticles (20)

2.1.2 Active Targeting

Active targeting is vital for effective drug delivery by modifying molecular ligands, such as antibodies, that directly attach to components like polymers (21). This method employs the surface molecules of nanoparticles to locate and bind to precise cells at targeted sites, enhancing the accuracy of drug delivery (22). Active targeting is divided into four categories: antibody-based, aptamer-based, peptide-based, and small-molecule-based targeting (23). In vivo, nanoparticle targeting initially takes advantage of the EPR effect before reaching the specific tumor site via a bypass pathway through surface modifications (24).

Representative ligands on the nanocarrier's surface are essential to ensure effective binding at the target site (25). A range of biological ligands has been identified and studied to enhance the active targeting of nanoparticles (NPs) (26). These ligands bind to specific receptors on target cell surfaces, increasing cellular uptake of drug-loaded NPs and boosting their therapeutic impact (27). Nanoparticles can be functionalised with these ligands primarily via chemical conjugation, physical adsorption after NP formation, or by linking them with components like polymers before NP synthesis (30). While nucleic acids, such as RNA, are often investigated as biological ligands, their quick dissolution in biological environments presents a notable challenge (31). Polymer-based nanoparticles, including aptamers, may mitigate this issue by offering benefits such as biodegradability, low toxicity, and reduced immunogenicity (32).

2.2 NANOPARTICLES

2.2.1. Definition and Properties of Nanoparticles

The International Organisation for Standardisation (ISO) defines nanoparticles (NPs) as nano-objects with dimensions typically ranging from 1 to 100 nm, characterized by slight differences between their longest and shortest axes (33).

These particles exhibit diverse shapes, including spherical, cylindrical, conical, tubular, hollow-core, spiral, and irregular geometries (34). Nanoparticles can be crystalline—either single-crystal or polycrystalline—or amorphous, and may exist as isolated particles or clusters (36, 37). Structurally, NPs may consist of a core, a chemically distinct shell, and a surface layer that can incorporate small molecules, metal ions, surfactants, or polymers (38).

2.2.2. HISTORICAL CONTEXT OF NANOTECHNOLOGY

Before understanding biotechnology, ancient civilizations were unaware that some of their techniques utilized nanoscale materials (39). A notable example is the dyeing of black hair in ancient Egypt. While traditionally believed to rely on plant-based substances like henna, recent analyses of hair samples from Egyptian tombs revealed the use of a mixture of lime, lead oxide, and water, which produced galena (PbS) nanoparticles (41, 42). This reaction between the paste and sulfur in keratin enabled uniform and long-lasting coloration.

Another remarkable early example of nanotechnology is the Lycurgus Cup from the fourth century CE (43). This Roman artifact displays different optical properties depending on light conditions—appearing green in natural light and deep red when lit from within (44). Spectroscopic studies attribute this effect to gold and silver nanoparticles embedded in the glass, which interact with light through electron plasmon excitation—a phenomenon foundational to modern nanotechnology (46).

2.2.3 Modern Nanoparticle Synthesis and Applications

In recent years, the synthesis of nanoparticles has increasingly embraced biological routes using plants and microorganisms. This approach offers an environmentally friendly and less hazardous alternative to traditional chemical or physical methods, which are often costly and energy-consuming. (47) Interdisciplinary collaborations among scientists from various fields have become essential in optimising nanoparticle production and characterisation.

Nanotechnology facilitates the fabrication of materials at the nanoscale, and nanoparticles (NPs) can be categorised based on their dimensional structures, ranging from 0D to 3D. Their nanoscale size significantly influences their physical and chemical properties, particularly optical features. For instance, metal nanoparticles exhibit colour variations depending on size:

Metal nanoparticle systems exhibit characteristic optical properties depending on their elemental composition and size, which are often reflected in their distinctive colors. For instance, gold nanoparticles (AuNPs) typically display a wine-red color due to strong surface plasmon resonance at the nanoscale. Platinum nanoparticles (PtNPs) are usually yellowish-gray, while silver (AgNPs) and palladium (PdNPs) nanoparticles appear black and dark black, respectively. These color variations not only serve as visual indicators of successful nanoparticle synthesis but also reflect differences in their electronic structures, surface properties, and potential biomedical applications.

These colour differences directly impact their absorption behaviour, making them especially useful for bioimaging applications (48).

2.2.4. Classification of Nanoparticles (NPs)

Graphene, as one of the earliest identified two-dimensional (2D) materials, has significantly influenced subsequent research in the field of nanomaterials (49). Its remarkable mechanical and electronic properties have inspired numerous studies, particularly in energy conversion and storage applications. Among 2D nanomaterials, nanocrystalline titanium dioxide (TiO_2) coatings stand out due to their favourable chemical stability and mechanical strength, making them prime candidates for hard tissue replacements (50). Additionally, self-assembled monolayers (SAMs)—organic molecules that spontaneously form ordered layers on solid surfaces—are widely utilized in biosensor technologies, enhancing sensitivity and specificity.

Quantum dots represent nanoscale semiconductor crystals capable of efficient electron transport and unique photoluminescent properties, emitting various colors upon ultraviolet excitation (51). Microwave-assisted colloidal synthesis has emerged as an effective method for producing these materials with controlled size and optical characteristics. Due to these features, quantum dots find applications in solar energy devices, biomedical imaging, light-emitting diodes, photodetectors, and photocatalysis.

Nanostructures such as nanowires, nanofibers, and nanorods occupy a vital niche within two-dimensional nanoscale materials. Nanowires are instrumental in developing field-effect transistors, sensors, and lasers, whereas nanofibers serve critical roles in tissue engineering, drug delivery, cancer diagnostics, and filtration systems (52). Nanorods, structurally solid analogs of nanofibers, are particularly valued for their superior performance in energy storage technologies.

Nanoparticles are broadly categorized based on their morphology, size, and chemical properties, each distinguished by specific physical and chemical characteristics (53).

2.1. CARBON-BASED NPS

2.2.5. Carbon-Based Nanoparticles

Fullerenes and carbon nanotubes (CNTs) represent two primary categories of carbon-based nanoparticles. Fullerenes are spherical carbon structures composed of pentagonal and hexagonal units, known for their electrical conductivity, high tensile strength, and structural resilience. Due to these properties, they have gained considerable interest in fields like electronics and nanomedicine. CNTs, on the other hand, consist of rolled graphene sheets and possess excellent mechanical, electrical, and thermal properties, making them valuable for sensors, drug delivery, and energy storage applications (54).

2.2.6. Metal Nanoparticles

Metal nanoparticles, particularly those derived from noble and alkaline metals such as gold, silver, and copper, exhibit unique optoelectronic properties due to localised surface plasmon resonance (LSPR). Their size, shape, and surface structure directly influence absorption behaviors in the visible spectrum, which is why they are widely utilized in biosensing, photothermal therapy, and imaging technologies. Gold nanoparticles, for example, are frequently employed in microscopy and as contrast agents due to their excellent conductivity and biocompatibility (55).

2.2.7. Ceramic Nanoparticles

Ceramic nanoparticles are inorganic, non-metallic materials produced via controlled thermal processes. They may be amorphous or crystalline and possess high thermal stability and chemical resistance. These features make ceramic NPs ideal for applications in catalysis, environmental remediation, and biomedical imaging. Titanium dioxide (TiO_2) and zinc oxide (ZnO) nanoparticles are among the most commonly studied types due to their photocatalytic and antibacterial activities (56).

2.2.8. Semiconductor Nanoparticles

Semiconductor nanoparticles bridge the gap between metals and insulators and exhibit size-dependent optical and electronic characteristics. With tunable bandgaps, they are particularly suited for applications in optoelectronics, photocatalysis, and energy harvesting devices. For example, cadmium selenide (CdSe) and zinc sulfide (ZnS) nanoparticles have shown promise in light-emitting and water splitting technologies(57).

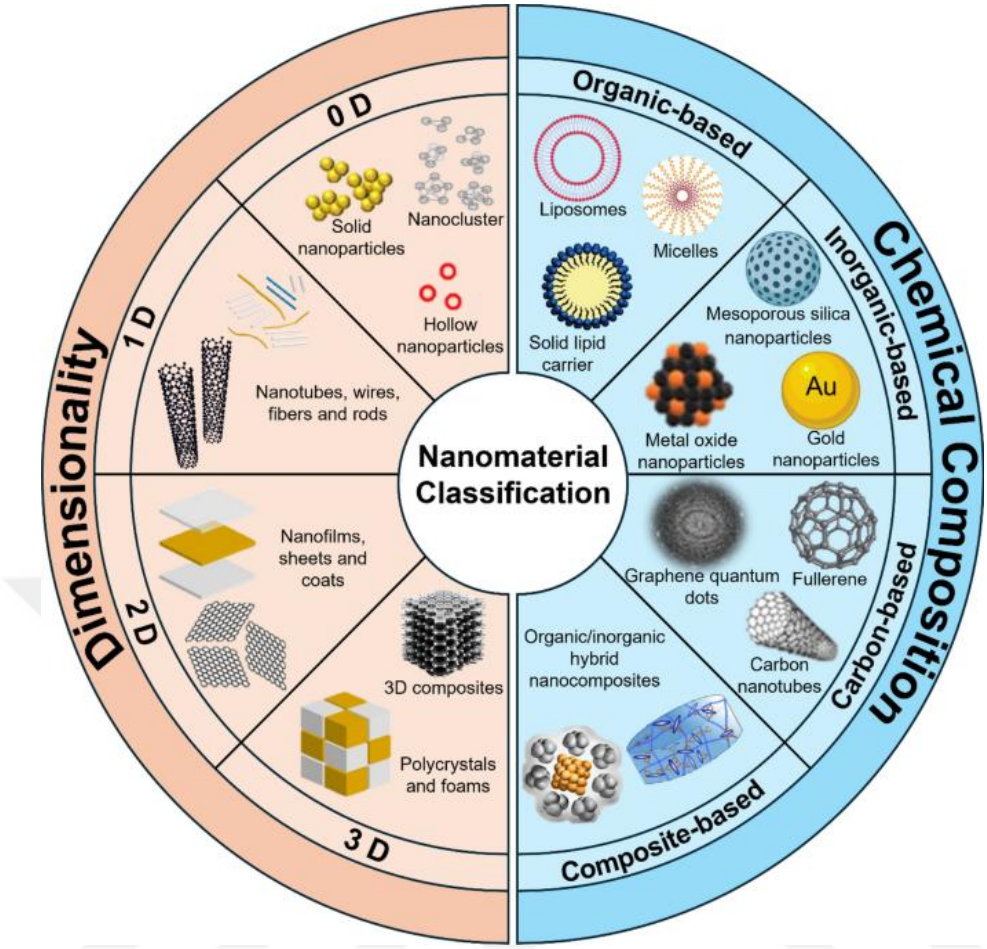

Figure 2.3. Different types of nanoparticles depending on their dimension/composition

2.2.9. Lipid-Based Nanoparticles

Lipid-based nanoparticles are composed of biocompatible lipid molecules and are especially significant in biomedical applications. Typically ranging from 10 to 1000 nm in diameter, they are used for delivering hydrophobic drugs or nucleic acids. Their core-shell structure—comprising a lipid core stabilized by surfactants—enables them to encapsulate active molecules effectively. Recent advances in lipid nanotechnology have led to breakthroughs in RNA-based therapies, especially in cancer and vaccine development (58).

2.2.10. Polymeric Nanoparticles

Polymeric nanoparticles (PNPs) are solid colloidal systems fabricated from natural or synthetic polymers. They are generally divided into two types: nanospheres, in which the drug is uniformly distributed throughout the matrix, and nanocapsules, which encapsulate the drug within a defined core. Their biocompatibility, controlled release capabilities, and tunable properties make them ideal candidates for targeted drug delivery, including across the blood–brain barrier. Polymers such as PLGA and PLA have been widely explored as non-viral vectors in gene therapy due to their ability to protect genetic material and provide sustained release (59).

Polymeric nanoparticles (PNPs) are generally classified into two main structural types**:** nanospheres and nanocapsules. In nanospheres, the therapeutic agent is uniformly dispersed throughout the polymeric matrix, forming a solid colloidal structure. In contrast, nanocapsules act as reservoir systems in which the drug is enclosed within a polymeric shell surrounding a core. This distinction is important in determining drug release behaviour, stability, and targeting capabilities of nanoparticulate delivery systems (60,61).

Depending on the synthesis method, drugs can be physically entrapped, chemically bound, or adsorbed onto the polymer matrix. Controlled drug release occurs either through diffusion across the polymer matrix or degradation of the polymer itself (62). Nanoparticles based on PLGA and PLA have been extensively investigated as nonviral gene delivery vectors due to their biocompatibility, biodegradability, sustained release properties, and ability to protect DNA from enzymatic degradation (63). Furthermore, smaller particle sizes and uniform distribution have been shown to enhance gene delivery efficiency (64).

The choice of polymer materials significantly influences the performance of nanoparticle formulations. Functionalized polymers are increasingly utilized to optimize the efficacy of polymeric nanoparticles. Biodegradable PNPs consist of naturally or synthetically derived polymers that break down into non-toxic byproducts within biological environments (65). These nanoparticles are highly

regarded for their biocompatibility, controlled drug release capacity, and their effectiveness in safeguarding therapeutic agents from enzymatic degradation (66). Common biodegradable polymers include poly(lactic-co-glycolic acid) (PLGA), polylactic acid (PLA), polycaprolactone (PCL), as well as natural polymers like chitosan and alginate (67).

The degradation rates and physicochemical properties of these polymers can be tailored to achieve sustained or targeted drug release, making them suitable for various biomedical applications (68). Biodegradable PNPs have attracted significant attention in drug delivery, gene therapy, and vaccine development due to their safety profile, adaptability, and ability to cross biological barriers such as the blood-brain barrier. Their properties also facilitate nonviral gene delivery by providing sustained release and protection of nucleic acids, thereby enhancing site-specific delivery while minimizing systemic toxicity (69).

2.3.1. Polymeric Micelles

Polymeric micelles are colloidal carriers composed of self-assembled block copolymers forming a core-shell architecture (70). Typically prepared from PLA-based polymers like PLGA, these micelles represent one of the most advanced and promising drug delivery systems. Engineering the block copolymers allows precise control over crucial parameters such as particle size, drug loading capacity, and release kinetics (71). Micelle formation occurs spontaneously when the critical micelle concentration and critical micellization temperature are exceeded (72). Below these thresholds, the polymers remain soluble; above them, hydrophobic interactions induce aggregation and micelle assembly.

The hydrophobic blocks constitute the inner core that encapsulates hydrophobic drugs, whereas the hydrophilic blocks create the outer shell, stabilizing the structure in aqueous environments (73). Studies have shown that polymeric micelles exhibit unique biodistribution profiles, making them well-suited for targeted drug delivery applications. Effective drug loading requires a solid core; otherwise, premature drug

release may occur (74). Additionally, the stability of polymeric micelles is influenced by factors such as drug charge density and polymer chain length (75). The chemical composition of the polymer primarily determines micelle size, which is generally independent of the preparation method, providing an advantage over other nanoparticle systems.

Recently, functionalized poly(ethylene glycol) (PEG) shells have been developed to facilitate receptor-mediated delivery of drugs and genes, while minimizing nonspecific interactions with serum proteins through PEG conjugation with targeting ligands (76).

2.3.2. PEG-PLGA-Based Nanoparticles

Polymer-based long-acting injectable formulations have significantly advanced drug therapy by offering sustained and predictable drug release over weeks to months, thereby enhancing patient adherence and convenience (77). Among the most frequently used biodegradable polymers in this context is poly(lactide-co-glycolide) (PLGA), a copolymer formed from lactic and glycolic acid monomers (78). PLGA exhibits excellent biocompatibility and has been approved by regulatory authorities such as the U.S. Food and Drug Administration (FDA) and the European Medicines Agency (EMA) for various medical applications (79).

Its degradation rate and drug release profile can be precisely controlled by modifying factors such as the monomer ratio, molecular weight, and the nature of the polymer end groups (80). These characteristics have made PLGA widely used in nanoparticle-based drug delivery systems designed for controlled and targeted therapeutic applications (80).

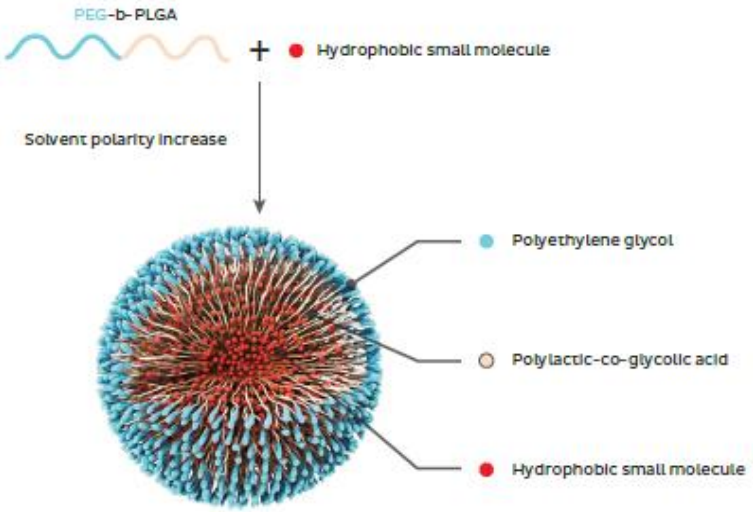

Figure 2.7. PEG-PLGA Based Nanoparticle

2.3.3. PEG–PLGA Nanoparticles: Transition and Functional Role

The shift from microparticles to nanoparticles in PLGA-based drug delivery marks a rational progression, given the superior advantages offered by nanoparticles (81). These include enhanced cellular uptake, improved bioavailability, and the ability to traverse biological barriers such as the blood–brain barrier. Nanoparticles can be precisely engineered to encapsulate a wide range of therapeutic agents, including small molecules, peptides, proteins, and nucleic acids. Block copolymers—especially combinations of PLGA with polyethylene glycol (PEG)—play a pivotal role in nanoparticle design due to their increased colloidal stability, prolonged systemic circulation, and decreased immune detection (82). The hydrophilic PEG shell provides a "stealth" effect, extending circulation time by minimising opsonisation and clearance by the mononuclear phagocyte system (83).

PEG is a non-ionic, hydrophilic polymer commonly employed to enhance the solubility and stability of nanoparticle drug carriers. It is synthesised via the polymerisation of ethylene oxide and is available in diverse molecular weights and structural architectures—both linear and branched. The molecular weight of PEG significantly influences its physicochemical behaviour and interaction with biological systems (84). Pegylation—the covalent linkage of PEG to drug molecules

or nanoparticles—has been widely applied to modulate pharmacokinetics, reduce immunogenicity, and improve drug retention in systemic circulation (85).

The application of PEG in biomedicine dates back to 1977, when it was first conjugated to proteins such as bovine serum albumin and liver catalase, yielding increased stability and reduced immune recognition. Since then, PEGylation has played a crucial role in PEG–PLGA nanoparticle systems, facilitating the controlled release of biomolecules like proteins and peptides. These systems are foundational in the development of nanomedicines for cancer therapy, gene delivery, and vaccine platforms. Functionalised PEG chains with targeting ligands have demonstrated improved cellular uptake and enhanced therapeutic specificity, particularly in cancer applications (86).

Despite its broad use, concerns have been raised about PEG-induced immunogenicity—a phenomenon termed the "PEG dilemma"—which may lead to the development of anti-PEG antibodies, thereby compromising therapeutic efficacy. Consequently, alternative stealth polymers such as poly(2-oxazoline) (POx) and zwitterionic materials are under active investigation. Nonetheless, PEG remains the most widely used hydrophilic polymer in nanoparticle drug delivery systems, owing to its excellent safety record and well-established efficacy (87).

2.4 FUNCTIONALIZATION METHODS

2.4.1. Surface Modification Strategies

Surface biomodification of nanostructures offers numerous advantages, such as biocompatibility, enhanced cellular internalisation, effective intracellular distribution, colloidal stability, regulated assembly, stealth capabilities, and target specificity (88). Furthermore, biological modification improves noninvasive, anticorrosive, anti-agglomerative properties and superior physical traits. The interactions between biomolecules and nanomaterials can be fine-tuned by adjusting surface properties like chemistry, charge, morphology, and nanoscale dimensions.

Physical adsorption is the most direct method for surface functionalisation, eliminating the need for extra strategies or reagents (89). However, it has its downsides, primarily due to the random orientation of bioreceptors on the surface. For example, citrate–capped gold nanoparticles (AuNPs) generally possess a negatively charged surface, allowing for electrostatic interactions with positively charged amino groups of biomolecules in solution.

Noncovalent binding involves weak attractive forces between polar and covalently bonded atoms across different compounds. These interactions facilitate surface functionalisation without altering the nanomaterial's underlying structure, resulting in a more straightforward and versatile process (90). Noncovalent interactions rely on electrostatic forces rather than electron transfer. The key advantages of noncovalent connections include the preservation of structural integrity and the maintenance of electrical characteristics. Despite their weak nature and low energy, noncovalent bonds are essential for upholding the stability of proteins and the three-dimensional structures of nucleic acids. This noncovalent surface modification technique has distinct benefits over direct covalent bonding (91). The active surface layer of noncovalently bound ligands can be removed, regenerated, and modified with appropriate solvents, thereby allowing the costly nanostructured sorbent to be reused and recycled. Research has shown that these noncovalent interactions can bestow novel properties onto nanomaterials while retaining essential characteristics; for instance, the sp^2 carbon networks remain intact during the noncovalent binding of carbon nanotubes (CNTs), ensuring that the material's structural features stay unaffected while advantageous properties are preserved (92).

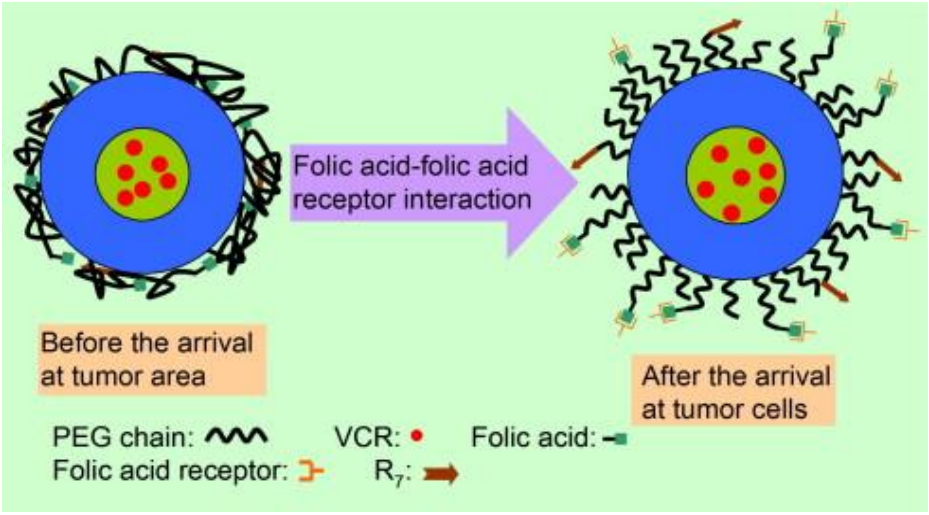

Figure 2.8 Chemistry of Surface Modification

Covalent binding is another widely used method for securing bioreceptors on substrate surfaces. (93) This process involves sharing electron pairs between atoms, establishing a stable balance between repulsive and attractive forces of the binding molecules (94). The desired molecules can be directly attached to reactive ligands on the substrate surface through covalent conjugation, assuming compatible functional groups are present. This approach irreversibly immobilises target molecules on the substrate, significantly enhancing the durability of the coatings (95).

Additionally, using a linker for covalent coupling minimises steric hindrance and its effect on the tertiary structure of the conjugated protein. In covalent attachment, nanoparticles are usually linked to receptors via initial functionalisation of the nanoparticle surface with linkers that interact with natural functional groups present on the biosensor structure (such as amine, carboxyl, or glycosyl groups) (96). This method modifies the substrate's surface characteristics while preserving its bulk composition, offering better control over bioreceptor orientation and overcoming most challenges of physisorption, such as poor orientation and steric hindrance (97).

2.4.2 PEGYLATION

PEGylation is the term that describes the modification of biological molecules by covalent conjugation with polyethene glycol (PEG). PEG is a non-toxic, non-immunogenic polymer, and is used as an advantage to overcome the disadvantages associated with biomaterials (98). PEGylation changes the chemical and physical properties of the biomedical molecule, such as its conformation and hydrophobicity, and improves the drug's pharmacokinetic behaviour. Generally, PEGylation improves drug solubility and drug stability and decreases immunogenicity and proteolysis, which allows reduced dosing frequency.

Various therapeutic proteins, antibody fragments and peptides, and small-molecule drugs have been PEGylated to benefit from these helpful pharmacokinetic impacts. Different properties of the PEG polymer, like mass, the site of PEG attachment, and the number of linking chains, have been shown to affect the biological activity and bioavailability of the PEGylated product. Releasable PEGs have been developed to slowly release the native protein from the conjugates into the blood. This aims to avoid any loss of efficacy that may occur with stable covalent PEGylation (99).

The first PEGylated drug was developed in the 1970s, and since then, PEGylated therapeutic agents have significantly improved the treatment of several diseases. Generally recognised as foreign objects, NPs are readily cleared from systemic circulation by the cells. However, PEG coatings on NPs shield the surface from accumulation, opsonisation, and phagocytosis, which prolongs NPs' circulation time.

Because of their hydrophilic properties, PEG chains attached to nanoparticles (NPs) create a hydrated layer with a significant excluded volume. This layer sterically inhibits interactions between NPs and both adjacent NPs and blood components. The enhanced permeability and retention (EPR) effect offers long-circulating PEGylated NPs a distinctive advantage for targeting tumors after systemic administration.

PEGylation conjugation techniques can be classified into two categories: (a) first-generation random PEGylation, and (b) second-generation site-specific PEGylation. Second-generation PEGylation processes can result in well-defined conjugated products with improved product profiles over those obtained through nonspecific random conjugations (100).

A reversible (or releasable prodrug) PEGylation concept has been formulated to minimise activity loss. The idea deals with drugs' attachment to PEG derivatives through cleavable linkages. Therapeutic agents release the drug through enzymatic, hydrolytic cleavage, or reduction in vivo at a predetermined kinetic rate.

Most PEG conjugation techniques aim to increase the circulation half-life without affecting activity. The distinct advancements in the PEG conjugation processes and diversity, like the PEGs used for the conjugation, have contributed to the increased demand for PEGylated pharmaceutical products. PEGylation enhances the therapeutic potency of drugs by bringing several advantageous modifications over non-PEGylated products.

PEGylation enhances the circulation time of conjugated therapeutics by improving their hydrophilicity and decreasing the glomerular filtration rate. It has also been noted that PEGylation increases the absorption half-life of agents administered subcutaneously and is linked to a reduced volume of distribution. PEG is a non-biodegradable polymer, which limits its application. Studies show that PEGs with a molecular weight of up to 20 kDa are mainly excreted through the renal system, while higher molecular weight PEG chains are eliminated via fecal excretion (101).

However, PEGylation brings certain drawbacks for liposomes, particularly regarding the delivery of genes and nucleic acids in anti-cancer therapies. Its hydrophilic surface shield decreases cellular uptake, enhances lipid envelope stability, and results in poor endosomal escape and degradation of cargo in lysosomes. Therefore, using PEG for gene and nucleic acid delivery in cancer cells

is termed the "PEG dilemma." This problem can be effectively tackled by developing pH-sensitive and tumor-specific targeted PEGylated therapeutics (102).

2.4.2. CONJUGATION VIA CHEMICAL COUPLING

The precise delivery of genes and drugs to tissues with high folate receptor (FR) expression attracts considerable interest (103). FRs are glycosylphosphatidylinositol-anchored proteins that show low levels in most normal tissues but significantly increase in various tumors, especially epithelial cancers. Ovarian cancer is a prominent example, with research indicating that over 90% of epithelial ovarian carcinomas display elevated FR-α levels. As ovarian cancer is among the deadliest gynecological cancers, targeting FRs offers a promising strategy to enhance therapeutic effectiveness by increasing tumor selectivity and reducing systemic toxicity.

In nanoparticle (NP) drug delivery systems, folic acid (FA) is often covalently attached to polymeric carriers like PEGylated poly(lactide-co-glycolide) (PEG-PLGA) using various chemical coupling techniques. These include carbodiimide-mediated (EDC/NHS) conjugation, thiol-maleimide reactions, or click chemistry.

This covalent bond enables receptor-mediated endocytosis, which enhances cellular uptake in tumors that overexpress folate receptors, such as ovarian cancer. By improving the internalisation of NPs in cancer cells, FA conjugation boosts the effectiveness of drugs, especially chemotherapeutic agents like paclitaxel and cisplatin, which are frequently employed in treating ovarian cancer.

2.5 OVARIAN CANCER

Ovarian cancer ranks among the deadliest gynecological cancers, primarily due to its diagnosis at advanced stages, high recurrence rates, and limited treatment options. While it is less common than breast or cervical cancer, its aggressive characteristics result in a grim outlook and elevated mortality rates (103). The typical first-line treatment for advanced ovarian cancer usually consists of cytoreductive surgery followed by platinum-based chemotherapy, including cisplatin or carboplatin, often paired with taxanes like paclitaxel. Although many patients see

positive responses initially, most face a recurrence of the disease within three years, requiring repeated chemotherapy cycles and further surgical procedures. Recurrent ovarian cancer often becomes resistant to standard chemotherapy, presenting a significant challenge in clinical oncology.

The BRCA1 and BRCA2 genes are well-known tumor suppressors that play a crucial role in the development of ovarian cancer. Germline mutations in these genes significantly increase the lifetime risk of developing ovarian cancer and affect treatment responses. Importantly, carriers of BRCA1/2 mutations with epithelial ovarian cancer show heightened sensitivity to platinum-based chemotherapy due to disruptions in homologous recombination repair (HRR). This realisation has prompted a shift towards targeted therapeutic approaches, especially poly (ADP-ribose) polymerase (PARP) inhibitors, which exploit DNA repair deficiencies in cancer cells. These inhibitors, like olaparib and niraparib, inhibit PARP enzymes, hindering the repair of single-strand DNA breaks, ultimately leading to synthetic lethality in HRR-deficient tumors. Despite their effectiveness, resistance to PARP inhibitors can still develop, highlighting the need for innovative drug delivery systems that improve therapeutic efficacy and minimise side effects (104).

One promising strategy in treating ovarian cancer is using nanotechnology-based drug delivery systems, particularly polymeric nanoparticles. Folate receptors (FRs), which are overexpressed in more than 90% of epithelial ovarian carcinomas, present a valuable target for ligand-mediated drug delivery. FA-conjugated nanoparticles can boost tumor specificity by promoting receptor-mediated endocytosis, enhancing drug accumulation in malignant tissues while lessening the impact on normal cells. Polymeric nanoparticles, such as PEG-PLGA formulations, offer further benefits, including better drug solubility, extended systemic circulation, and controlled drug release. PEGylation provides a protective hydrophilic shell that reduces opsonization and rapid clearance, thus extending systemic circulation and enhancing nanoparticle accumulation in tumor tissue.

2.5.1. Targeted and Non-Targeted Approaches for Ovarian Cancer

In recent years, the need for more effective and selective treatments for ovarian cancer has prompted the development of advanced drug delivery platforms. Nanoparticle-based systems—particularly those utilizing PEG–PLGA polymers—have demonstrated great potential due to their tunable properties, biocompatibility, and ability to carry various therapeutic agents. One of the most promising strategies involves the use of targeted nanoparticles, particularly those functionalized with folic acid (FA), which actively bind to folate receptors (FRs) overexpressed in more than 90% of epithelial ovarian carcinomas. These FA-conjugated nanoparticles leverage receptor-mediated endocytosis to selectively enter cancer cells, thereby enhancing drug accumulation in tumors while reducing off-target effects. The presence of a PEG shell not only minimizes recognition by the immune system but also prolongs systemic circulation, enabling enhanced tumor penetration via both passive (EPR effect) and active (ligand-receptor binding) targeting mechanisms. For instance, FA-decorated PEG–PLGA nanoparticles loaded with genistein or co-loaded with docetaxel and gemcitabine have demonstrated enhanced cytotoxicity and tumor suppression with minimal systemic toxicity in preclinical models (105).

Conversely, non-targeted nanoparticles, which rely solely on the Enhanced Permeability and Retention (EPR) effect, also present a viable therapeutic approach. These nanoparticles passively accumulate in tumor tissue due to leaky vasculature and impaired lymphatic drainage commonly observed in solid tumors. While they benefit from prolonged circulation time and reduced renal clearance due to PEGylation, the absence of active targeting may result in lower cellular uptake and higher systemic drug distribution. This limits their specificity and therapeutic index compared to FA-targeted counterparts. Nevertheless, non-targeted PEG–PLGA systems have shown notable antitumor effects and remain relevant, especially in cases where FR overexpression is inconsistent or targeting ligands may induce immune responses.

In conclusion, both targeted and non-targeted polymeric nanoparticles offer unique advantages in the context of ovarian cancer treatment. While FA-targeted nanoparticles clearly outperform in terms of tumor selectivity and therapeutic efficacy, non-targeted systems provide a more generalized approach that still enhances drug pharmacokinetics and reduces toxicity. As research advances, optimizing parameters such as ligand density, particle size, and drug loading efficiency will be essential for translating these strategies into clinical settings.

2.5.2. FA in Ovarian Cancer

Folic acid is critical in various biological processes, including DNA synthesis, repair, and methylation, making it essential for cell growth and division. It can be added to NP formulations through non-covalent techniques like physical adsorption or encapsulation, potentially providing simpler alternatives while facilitating receptor-mediated uptake. In PEG-PLGA-based NP systems, the PEG shell minimises non-specific interactions, extending systemic circulation, and enhancing tumor accumulation through the enhanced permeability and retention (EPR) effect. This combination of active targeting (FA-mediated) and passive targeting (EPR-based) delivers a dual benefit by increasing drug delivery precision and reducing off-target effects (106).

With the pressing need for more effective treatments for ovarian cancer, folate-functionalized nanoparticles represent a promising avenue for targeted drug delivery, particularly in addressing drug resistance and improving the efficacy of chemotherapy. Ongoing research is focused on refining these delivery systems to optimise ligand density, polymer composition, and nanoparticle size for maximum tumor penetration and therapeutic effectiveness.

2.5.1. DNA Damage and Repair Mechanisms

Cellular survival largely depends on preserving the genetic code, which constantly faces threats from internal and external DNA-damaging agents. Internal sources include reactive oxygen species (ROS) generated during normal metabolic

activities, while external factors such as ultraviolet (UV) radiation, ionising radiation, and chemical mutagens further challenge genomic stability. To maintain integrity, cells employ various DNA repair pathways, including single-strand break repair (SSBR), base excision repair (BER), nucleotide excision repair (NER), and homologous recombination (HR) (106). These mechanisms correct DNA damage, prevent mutation accumulation, and protect against diseases like cancer. Failures in repair processes lead to genomic instability, which is a hallmark of tumorigenesis. Given their critical role, DNA repair pathways have become promising therapeutic targets; inhibitors of specific repair enzymes can selectively target cancer cells, improving treatment efficacy (107).

Among these pathways, the Base Excision Repair (BER) mechanism is vital for correcting small base lesions caused by oxidative stress, alkylation, and spontaneous hydrolytic reactions. BER is initiated by DNA glycosylases that recognize and excise damaged bases, followed by AP endonuclease (APE1) generating a single-strand break. DNA polymerase β and DNA ligase III subsequently fill in and seal the gap to complete the repair process (108). Ineffective BER can lead to mutagenesis and contribute to genomic instability, underlining its importance for cellular health and cancer prevention.

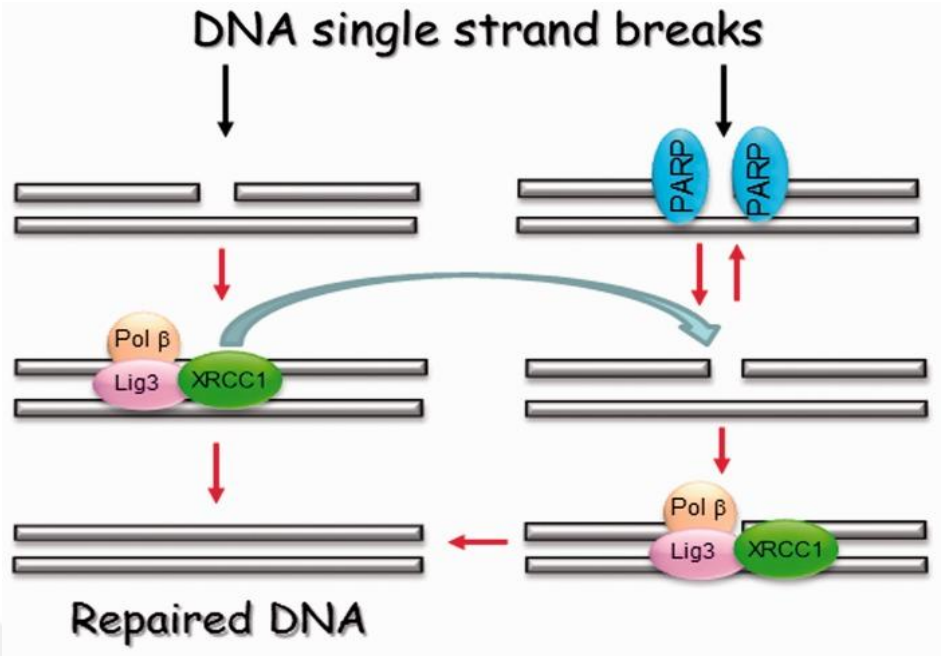

Figure 2.10 PARP's effects on DNA Break

A significant regulator of BER is the poly (ADP-ribose) polymerase (PARP) family, especially PARP1 and PARP2, which are vital in recognising and repairing DNA strand breaks. When DNA damage occurs, PARP1 binds to the damaged site and facilitates the addition of poly (ADP-ribose) (PAR) chains through PARylation . This modification helps resolve the damage by recruiting additional repair factors, such as XRCC1. Moreover, PARP1 stabilises replication forks and mitigates DNA replication stress, contributing significantly to genomic integrity. (109)

In cancer treatment, targeting the BER pathway via PARP inhibition has proven to be an effective strategy, particularly for tumors with homologous recombination repair (HRR) deficiencies, such as those caused by BRCA1/2 mutations in ovarian and breast cancers (110). PARP inhibitors (PARPi), like olaparib, niraparib, and rucaparib, induce synthetic lethality by trapping PARP1 at the sites of DNA damage, hindering repair efforts and resulting in irreversible DNA breaks (110). This targeted toxicity is particularly lethal to HR-deficient cancer cells while sparing normal cells, leading to reduced systemic toxicity compared to standard chemotherapy (110).

The advent of nanoparticle-based delivery systems, such as PEG-PLGA nanoparticles, has enhanced the clinical effectiveness of PARPi by improving drug solubility, extending systemic circulation, and enabling targeted tumor accumulation (111). By refining nanoparticle formulations, researchers aim to combat PARPi resistance and enhance treatment outcomes in HR-deficient cancers, especially ovarian cancer, where PARPi therapy has become a key treatment option (111).

A PARP inhibitor is a type of cancer treatment that inhibits PARP, which stands for “poly (ADP-ribose) polymerase.” This protein plays a crucial role; when a cell's DNA is damaged, PARP assists in its repair. These repairs are vital since DNA contains the genes that dictate how cells function correctly (112).

However, cancer cells can also utilise PARP to mend their DNA, enabling them to survive and proliferate (112). By administering a PARP inhibitor, cancer cells are deprived of this protein, ultimately leading to their death (112).

Several PARP inhibitors have been approved for clinical use by the U.S. Food and Drug Administration (FDA) and the European Medicines Agency (EMA), including olaparib (Lynparza®), niraparib (Zejula®), rucaparib (Rubraca®), and talazoparib (Talzenna®). These agents have become key components in the treatment of various cancers, particularly those associated with BRCA mutations and defects in DNA repair mechanisms.

2.5.2. 3. Aminobenzamide (3- AB) as a PARP Inhibitor

3- Aminobenzamide (3-AB) was one of the first recognised PARP-1 inhibitors, acting as a competitive inhibitor by binding to the enzyme's NAD+ site (113). PARP-1 is important in the Base Excision Repair (BER) pathway, aiding in DNA repair and preserving genomic integrity (113). By inhibiting PARP-1, 3-AB interferes with the DNA repair mechanism, accumulating DNA strand breaks and ultimately triggering apoptosis, especially in cancer cells with existing DNA repair deficits, such as those in BRCA-mued ovarian cancer (113).

Nonetheless, compared to modern PARP inhibitors like olaparib and niraparib, 3-AB has several drawbacks, including lower potency, rapid metabolism, and poor bioavailability (114). These pharmacokinetic limitations reduce its therapeutic potential, highlighting the need for alternative drug delivery strategies to boost effectiveness (114).

2.5.2.4. Nanoparticle-Based Delivery of 3-AB

To address these issues, nanoparticle encapsulation presents a promising solution. Polymeric nanoparticles, like PEG-PLGA nanoparticles, offer distinct advantages for delivering 3-AB:

Increased drug stability: Protects 3-AB from quick degradation and metabolism.

Controlled release: Provides sustained drug availability at the tumor location.

Enhanced tumor targeting: PEGylation improves circulation time, and including folate receptor targeting can increase uptake by tumor cells.

Reduced systemic toxicity: Limits non-specific drug distribution and off-target effects (111,114).

2.5.2.5.Potential Application in Ovarian Cancer Therapy

Since ovarian cancer cells often show homologous recombination (HR) deficiencies, especially in BRCA 1/2 mutation carriers, they are notably vulnerable to PARP inhibition approaches (110). 3-AB-loaded PEG-PLGA nanoparticles could offer a more effective and targeted treatment for ovarian cancer by ensuring prolonged drug retention at the tumor site while minimising premature clearance from the bloodstream (111). Additionally, combining 3-AB with other DNA-damaging agents, such as platinum-based chemotherapy (cisplatin, carboplatin), ATR inhibitors, or immune checkpoint inhibitors, could enhance its therapeutic efficacy and help overcome resistance mechanisms tied to single-agent PARP inhibition (112).

2.5.2.6. DNA Damage and Repair Mechanisms

In vitro models like the SK-OV-3 cell line are vital in understanding ovarian cancer biology and treatment responses. These cells, known for their epithelial structure, demonstrate resistance to tumour necrosis factors and various cytotoxic drugs, such as cisplatin and adriamycin. They have tumorigenic capabilities, forming colonies in soft agar and producing tumors that resemble clear cell adenocarcinoma when injected into immunocompromised mice (113).

Given the difficulties linked to PARP inhibitor resistance, exploring alternative drug delivery methods is essential. Encapsulating 3-Aminobenzamide (3-AB) within PEG-PLGA nanoparticles represents a promising strategy for improving drug stability, enhancing tumor targeting, and addressing the limitations of ovarian cancer treatments. As research advances, innovative nanoparticle formulations and combination therapies focused on DNA repair weaknesses hold considerable potential to enhance patient outcomes and address current obstacles in ovarian cancer management. (114)

3. MATERIALS AND METHODS

3.1 Materials

Poly(ethylene glycol) (PEG, Sigma Aldrich), poly(lactic-co-glycolic acid) (PLGA, Sigma Aldrich), acetone (99%, Merck), folic acid (Sigma Aldrich, USA), anhydrous dimethyl sulfoxide (DMSO, Sigma Aldrich, USA), Dulbecco's Modified Eagle Medium (DMEM, Gibco), DAPI (Thermo Fisher), Alexa Fluor 488 dye (Thermo Fisher), Amicon® Ultra Centrifugal Filter Units (MWCO: 100 kDa, Merck), 3-aminobenzamide (3-AB, Sigma Aldrich), tetrahydrofuran (THF, Merck), and acetonitrile (Merck) were used in this study.

Dynamic light scattering (DLS) and zeta potential measurements were performed using a ZetaSizer Nano ZS instrument (Malvern Instruments, UK). Drug loading and release were quantified using LC/MS-MS (Thermo Scientific). Cell viability assays were carried out using the GLPbio CCK-8 Kit (GLPBIO). Fluorescent imaging was performed using a microplate reader (Varioskan Lux, Thermo Scientific), a lyophilizer was used for nanoparticle drying (Labconco), and a NanoDrop spectrophotometer (Thermo Scientific) was used for concentration analysis.

3.2 Nanoparticle Preparation and Characterisation

3.2.1. Preparation and Characterisation of PEG-PLGA Nanoparticles

Generally, PEG–PLGA copolymers can be categorised into several structural types: A-A-A-B diblock, A–B–A or B–A–B triblock configurations, alternating multiblock formations, multi-armed designs, and star-shaped block varieties. The confirmation significantly affects their applications. Various PEG–PLGA copolymer structures with unique properties have been utilised in diverse drug delivery systems.

PLGA-PEG copolymer is made by PLGA-COOH (1 g, 0.0166 mmol) and the coupling agent DCC (17.4 mg, 0.042 mmol) that were dissolved in 2 mL of anhydrous DCM in a nitrogen atmosphere. Then, a solution containing hydroxyl-terminated PEG (66.6 mg, 0.033 mmol) and DMAP (3 mg, 0.012 mmol) was added to the mixture in anhydrous DCM (3 mL). After stirring for 2 hours at 1000 rpm, the reaction mixture was precipitated with cold diethyl ether and collected via suction filtration. The produced PLGA-PEG was characterised using 1H NMR and FT-IR spectroscopies and stored at +4 °C. (162)

Micelle Preparation using THF as solvent

PEG-PLGA Polymer solutions were prepared by dissolving the 20 kDa PEG-PLGA polymer. Five milligrams of PEG-PLGA were dissolved in THF and 1 mL of acetone (99%). The polymer solution was then added slowly to progress micelle formation. These micelle solutions were incubated in a shaker at 37 °C for 6 hours, then another two were made and incubated for 24 hours to ensure complete self-assembly and stabilisation of the micelles. During this incubation, solvent evaporation occurred, enhancing micelle integrity and homogeneity.

Micelle Preparation using Acetone as Solvent

For the optimal Peg-PLGA nanoparticle, 5 mg of Peg-PLGA (20 kDa) was dissolved in 1 mL of acetone (99%), which helped achieve even particle distribution. The solution was vigorously mixed using a vortex to improve dispersion. Next, the polymer solution was gradually added to 5 mL of distilled water while continuously stirring to encourage micelle formation. This micelle solution was incubated in a 37 °C shaker at 200 rpm for 24 hours to stabilise the nanoparticles.

3.1.1.1. Size Measurement for PEG-PLGA Micelles

The size distribution of the PEG-PLGA micelles was determined using Dynamic Light Scattering (DLS). To achieve this, the micelle solutions were diluted with distilled water in different ratios. The dilution series was carefully designed to ensure

accurate measurements and comprised the following ratios: 1:2, 1:4, 1:16, 1:32, 1:64, 1:128, 1:256, 1:512, and 1:1064. Each diluted sample was analysed to discover its hydrodynamic diameter, which provides valuable insights into the micelles' stability and uniformity in aqueous environments.

3.1.1.2. Zeta Potential Measurement of Empty Micelles

Zeta potential measurements were carried out to assess empty micelles' surface charge and colloidal stability. The analysis was done with PEG-PLGA micelles.

A 100 µl sample was diluted with 900 µl Sodium Chloride (NaCl) to achieve the proper concentration and analysed using a dynamic light scattering (DLS) zeta potential analyser (Malvern Zetasizer). The measurements were conducted at room temperature, and results were expressed in millivolts (mV). All experiments were performed in triplicate, and the mean values were taken.

3.1.3. Critical Micelle Concentration (CMC) of PEG-PLGA Micelles

The critical micelle concentration (CMC) of the PEG-PLGA copolymer needed was 10^-5 in 3 ml, specifically 62 kDa. This results in a required polymer concentration of 1,86mg. Next, 500 µl of pure acetone was added to dissolve the PEG-PLGA. It was diluted five times with 100 ml of stock solution and 400 ml of pure acetone. From a mixture of 5 ml of pyrene and 5 ml of acetone stock solution, 142,4 µl was added to the dilutions. After that, it was left to sit for 2 hours to allow the acetone to evaporate. Finally, 500 µl of acetone was added to the solutions, and they were left overnight. Absorbance values were measured using a Varioskan™ ultimode microplate reader, functioning in UV-Vis spectrophotometric mode, utilising pyrene as a hydrophobic fluorescent probe. Various concentrations of PEG-PLGA solutions were prepared with a constant amount of pyrene.

Absorbance was measured at 336 nm using a UV-Vis spectrophotometer. The CMC was determined by plotting the absorbance against the logarithm of polymer concentration and pinpointing the inflexion point on the resulting curve.

3.2.2. Preparation of Drug-Loaded Micelles (3-AB-MIC)

3.2.2.1. Preparation of Drug-Loaded Nanoparticles

Drug-loaded PEG–PLGA micelles containing 3-aminobenzamide (3-AB) were prepared using the solvent evaporation technique. PEG–PLGA polymer and 3-AB were dissolved together in acetone to obtain a homogenous organic phase. Three different concentrations of 3-AB (5%, 10%, and 20% w/w relative to the polymer) were tested to evaluate the effect of drug loading on micelle characteristics.

The organic mixture was slowly added dropwise into distilled water under continuous magnetic stirring. Due to the amphiphilic nature of the PEG–PLGA polymer, micelles formed spontaneously as the solvent diffused and evaporated. The resulting suspension was then incubated at 37 °C for 24 hours to ensure complete solvent removal and micelle stabilization.

To remove unencapsulated free drug and purify the micellar suspension, the mixture was transferred into Amicon Ultra centrifugal filters (MWCO: 10 kDa) and centrifuged at 4000 rpm for 30 minutes. The retained micelle fraction was collected, while the filtrate containing free 3-AB was discarded. This purification step was repeated three times using fresh distilled water to ensure complete removal of unbound drug molecules.

The purified micelle formulations were stored at 4 °C until further characterization and analysis.

3.2.2.2. Evaluation of Drug-Encapsulation Efficiency

To prepare the calibration curve, stock solutions of the 3-aminobenzamide compound were prepared at 5%, 10%, and 20% (w/v) concentrations in acetone. Each stock solution was then diluted with acetonitrile at a ratio of 1:2 (v/v), leading to ten serial dilutions for every concentration.

Absorbance measurements were performed using a NanoDrop spectrophotometer (Thermo Scientific) at 250 nm. The collected data were used to develop calibration curves, which were later applied to quantify drug content in micellar formulations.

3.2.2.3. Determination of Drug Release Profiles from Drug-Loaded Nanoparticles

To understand the time-dependent drug release profile of Fa-PEG-PLGA, the micelles were incubated in two different media: a 10 mM phosphate-buffered saline (PBS) solution at pH 7.4 to mimic the physiological conditions of healthy tissues, and a 0.1 mM acetate buffer solution at pH 5.5, which mimic the acidic inflammatory environment of cancerous tissues.

Each 1 mL of Fa-PEG-PLGA micelle solution was placed in a dialysis membrane (Molecular Weight Cut-off: 1 kDa). The dialysis system was immersed in 50 mL of buffer solution, and incubation was started. These dialysis systems were maintained at 37 °C and 150 rpm on an orbital shaker to ensure dynamic conditions similar to in vivo environments. At predetermined time intervals (1, 2, 4, 8, and 12 hours, followed by 1, 2, 4, 6, 8, 10, 12, and 15 days), 100 µL samples were taken from the dialysis medium and stored at -20 °C for further analysis. The collected samples were analysed using LC-MS/MS to determine the concentration of released folic acid, providing insight into the drug-loaded micelles' release kinetics and potential bioavailability.

3.2.3. Folic Acid-Attached PEG-PLGA Micelles

"Micelles were prepared using a mixed polymer strategy to achieve a 4% (w/w) folate functionalization. Specifically, 0.2 mg of FA–PEG–PLGA and 4.8 mg of PEG–PLGA (totaling 5 mg of polymer) were co-dissolved in 1 mL of acetone to obtain a homogeneous organic phase.This solution was slowly added to distilled water under constant stirring, promoting the spontaneous formation of micelles. The suspension was incubated at 37 °C for 24 hours to allow complete evaporation of the organic solvent and stabilization of the micelles.

The micellar formulations were then characterized to assess their physicochemical properties. Dynamic light scattering (DLS) was used to determine the average particle size and polydispersity index (PDI), while zeta potential measurements were performed to evaluate surface charge and colloidal stability under aqueous conditions.

This co-polymer system allowed the incorporation of folic acid functionality for targeted delivery, while PEG–PLGA provided structural integrity and optimized micelle formation.

Optimization of FA-PEG-PLGA Ratios

During the optimization studies, different weight ratios of FA–PEG–PLGA to total polymer (2%, 4%, and 10% w/w) were evaluated to determine the most stable micelle formulation. Based on preliminary characterization results including particle size distribution and stability, the 4% (w/w) ratio was selected for all subsequent loading and in vitro experiments due to its optimal targeting potential and physical stability.

3.2.2.3. Zeta Potential Measurement of FA-PEG-PLGA Micelles

Zeta potential measurements were carried out to assess FA-PEG-PLGA micelles' surface charge and colloidal stability. The analysis was done with FA-loaded PEG-PLGA micelles.

A 100 µl sample was diluted with 900 µl Sodium Chloride (NaCl) to achieve the correct concentration and analysed using a dynamic light scattering zeta potential analyser. The measurements were conducted at room temperature, and results were expressed in millivolts (mV). All experiments were performed in triplicate, and the mean values were acquired.

3.4. Preparation of Fluorescent Dye Conjugated Nanoparticle (Nile Red -PEG-PLGA Micelles)

Nile Red (ex552/em636) fluorescent dye was chosen as the imaging agent for preparing dye-conjugated micelles due to its strong hydrophobicity and stability in

lipophilic environments. The encapsulation of Nile Red within PEG-PLGA micelles enables efficient fluorescence-based tracking, making it a valuable tool for studying nanoparticle behaviour, cellular uptake, and biodistribution.

The fluorescent micelles were prepared using the solvent evaporation technique. PEG-PLGA (4,8 mg) and Nile Red (0,2 mg/ml) were dissolved in 1 mL of acetone to achieve homogeneity. The organic phase was then added slowly into 5 mL of distilled water under continuous stirring, promoting the self-assembly of micelles. The mixture was then incubated in a 37 °C shaker at 200 rpm for 24 hours to ensure the micelles' complete solvent evaporation and stabilisation.

To confirm successful Nile Red loading and evaluate the physicochemical properties of the micelles, several characterisation techniques were performed:

Dynamic Light Scattering (DLS): Employed to measure the hydrodynamic size and polydispersity index (PDI) of the micelles, ensuring uniformity.

The Nile Red-PEG-PLGA micelles were stored in a dark environment at 4°C to prevent photobleaching and degradation before further in vitro and in vivo studies.

3.5 IN VITRO EXPERIMENTS

3.5.1. Cell Preparation and Maintenance

SKOV-3 cancer cells and L929 Fibroblast cells were incubated in complete DMEM medium containing 10% FBS and 1% penicillin in a CO_2 incubator at 5% CO_2, 90% humidity and 37 °C. Cells were washed with 1X PBS and incubated in 0,25% trypsin-EDTA solution at 37 °C for 5 minutes. Afterwards, trypsin was deactivated with medium at room temperature, and the detached cells were collected and centrifuged at 500g for 8 minutes. After centrifugation, the supernatant was carefully discarded, and the cells were resuspended in the medium. For cell counting, 10 µL of

the thawed cell solution was mixed with trypan blue at a ratio of 1:2, and cells were counted on a hemocytometer using a light microscope.

3.5.2. Cytotoxicity Test

Cytotoxicity tests were performed using the Cell Counting Kit-8 (CCK-8, GLPBIO) on the human ovarian cancer cell line (SK-OV-3) and Mouse fibroblast cells (L-929). After cell counting, cells were seeded with 10,000 cells/100 μL medium in each well of a 96-well plate and incubated at 5% CO_2, 37 °C for 24 hours to allow cells to attach. The next day, after removing the medium from the cells, different groups of samples (empty nanoparticles and 3 AB) were prepared in various dilutions and were sterilised under UV for 15 minutes before mixing with media to get a total volume of 100 μL. This mixture was added to the cells. Wells with only media were blank controls, and wells with cells without treatment were positive controls. All samples were added to the wells in n = 3 replicates. The cells were then incubated at 5% CO_2, 37 °C for 24 hours. The next day, 10 μL of CCK-8 reagent was added to each well and incubated for 3 hours at 5% CO_2, 37 °C. After 3 hours of incubation, the results were obtained by a microplate reader at 450nm. And analysed with GraphPad.

3.5.3. Cell Internalisation Study

3.5.3.1. Cell Treatment and Fixation

Cell fixation was performed using Nile Red (Thermo Fisher) on the human ovarian cancer cell line (SK-OV-3).

After cell counting, cells were seeded with 10000 cells/500ul medium in 4 wells of 5 different incubation timed 24-well plates and incubated at 5% CO2, 37 °C for 24 hours to allow cells to attach. The next day, after removing the medium from the cells,

different groups of samples (Nile red, Nile Red Loaded Micelles and Nile Red Loaded FA-PEG-PLGA micelles) were sterilised under UV for 15 minutes before mixing with media to get a total volume of 500 μL. This mixture was added to the wells. Wells with cells without treatment were positive controls. All samples were added to the wells in n = 1 replicates. The cells were then incubated at 5% CO2, 37 °C for 24 hours.

Cells were fixated following this procedure; For the fixation of adherent cells, the phosphate-buffered saline (PBS) solution was first pre-warmed to 37 °C to prevent temperature-induced cellular stress. The culture medium was carefully aspirated from each well using a pipette. Cells were then gently washed with 1 mL of PBS per well, followed by a gentle rocking motion to ensure uniform removal of residual medium. The cells were incubated with PBS for 5 minutes to maintain isotonic conditions before fixation. After this incubation, PBS was aspirated and the cell monolayer was briefly inspected under the microscope to evaluate cell confluency and morphology. Subsequently, 1 mL of ice-cold 4% paraformaldehyde (PFA) was slowly added to each well to initiate chemical fixation. The fixation step was carried out for 10 minutes at room temperature. To minimize the risk of dislodging the cell layer, the removal of PFA was performed cautiously and gradually. A second visual inspection was conducted post-fixation to ensure cellular integrity and to check for any detachment or morphological damage. The fixed cells were then stored at 4 °C in PBS or appropriate buffer until further analysis.

3.5.3.2. Cell Staining

DAPI Stock Solution Preparation

DAPI powder (5 mg) was dissolved in 5 mL of 1× DPBS (pH ~7.4) to create a stock solution with a concentration of 1 mg/ml. The solution was divided into 1 mL aliquots: four were kept at –80 °C, while the remaining 1 mL was stored at –20 °C and marked as “in use.”

Staining with DAPI

Following 1–3 washes with 1× DPBS, a working DAPI solution was prepared at 4 µg/ml by diluting 12 µL of the 1 mg/ml stock into 3.0 ml of 1× PBS. 500 µL of this solution was added per well in a 24-well plate. Cells were incubated at room temperature for 1–5 minutes, protected from light. Subsequently, the staining solution was removed, and cells were washed 2–3 times with 1× DPBS before imaging.

Concanavalin A Alexa Fluor™ 488 Stock Solution Preparation

5 mg of Concanavalin A Alexa Fluor™ 488 conjugate was mixed in 5 mL of 0.1 M sodium bicarbonate buffer (pH ~8.3) to make a 1 mg/mL stock solution. This solution was divided into 1 mL aliquots: four portions were kept at –80 °C, while the remaining 1 mL was stored at –20 °C and marked as "in use."

Staining with Concanavalin A Alexa Fluor™ 488

The cells were washed 1–3 times with 1× DPBS. A working Concanavalin A Alexa Fluor™ 488 solution was prepared at a final concentration of 5 µg/ml by diluting 15 µL of the 1 mg/ml stock in 3.0 ml of 1× PBS. 500 µL of this staining solution was added to each well of a 24-well plate. Cells were incubated for 1 hour at room temperature, protected from light. After incubation, the staining solution was removed.

4. RESULTS

4.1 Nanoparticle Preparation and Characterisation

4.1.1. Preparation and Characterisation of PEG-PLGA Micelles

The PEG-PLGA copolymer was successfully synthesised, and various nanoparticle formulations were tested to identify the optimal preparation conditions. Parameters like polymer concentration, solvent type, and filtration method were adjusted to attain the best particle size distribution.

The synthesised PEG-PLGA was characterised using 1H NMR and FT-IR spectroscopy, confirming the copolymer's successful formation. The product was stored at 4°C. This refined PEG-PLGA structure served as the foundation for the ensuing micelle formation and drug loading experiments.

Micelles were prepared with a previously prepared PEG-PLGA copolymer. Acetone and TCF were chosen to dissolve PEG-PLGA because TCF and acetone are amphilic, which can dissolve both PEG and PLGA in a homogeneous solution. They also have low boiling points, making evaporating and forming micelles easier.

PEG-PLGA copolymers were added to 1 mL of THF and then dissolved by repeatedly mixing with a micropipette. After those solutions were added to 5 mL of distilled water and put into an orbital shaker to mix, the nanoparticles were incubated for 6 and 24 hours to check micelle preparation. Then, they were filtered using a PES filter (0,22 μm). The same experiment was done with acetone.

In further studies, THF was later discarded as a solution because it's thought that THF didn't evaporate enough in 6 and 24 hours, respectively. This is why it was decided to use acetone as a solvent and wait 24 hours for it to evaporate completely.

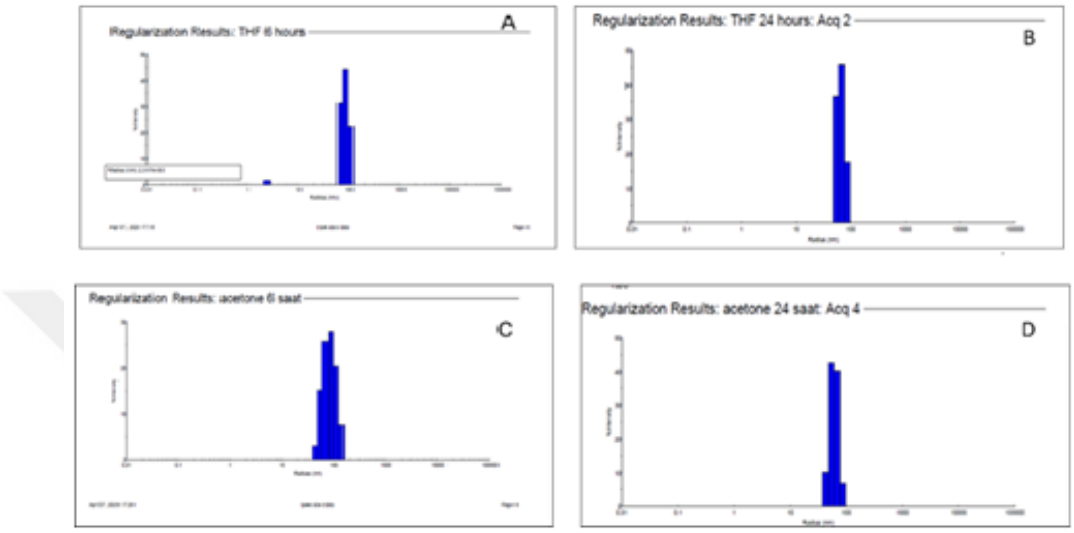

Figure 4.1. Effects of solvent on NP size at different time points. Comparison of nanoparticles prepared with THF and Acetone. The A and B are with THF in 6 hours and 24 hours. The C and D are with Acetone in 6 hours and 24 hours.

The experiments were performed simultaneously to optimise reaction time and dilution. First, the previously described procedure was repeated using acetone (99% Merck) with and without filtration. 5mg PEG-PLGA was dissolved in 1 ml of acetone and added dropwise to 5 ml of distilled water. Samples were prepared and incubated in an orbital shaker for 6 and 24 hours. Then, they were checked using DLS, filtered using a PES filter (0.22 μm), and measured with DLS again.

Subsequently, all prepared nanoparticles were filtered with 0,22 μm polyester sulfone (PES) filters, and the size was measured again with the DLS. The graphs in Figure 4.2

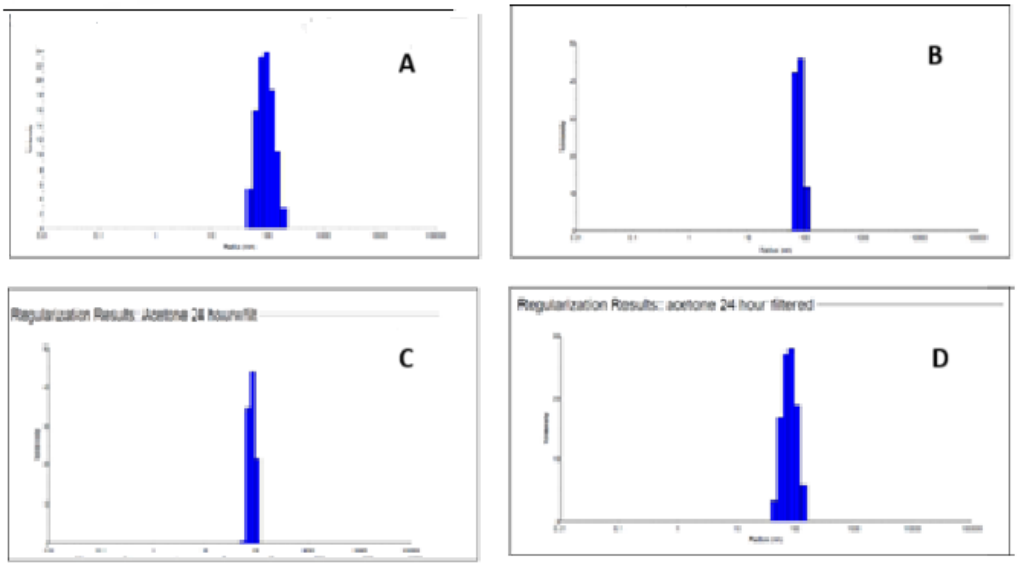

Figure 4.2. Effects of filtration on NP size at different time points. Comparison of nanoparticles prepared with Acetone. The A and B are Acetone in 6 hours without filtration and with filtration. The C and D are Acetone in 24 hours, without and with filtration.

Table 4.1. Effects of solvent on NP size at different time points.

Solvent	Diameter (nm)	PDI (%)
Acetone	168,82	29,66
THF	164,22	17,63
Acetone	121,64	18,28
THF	132,52	17,28

Table 4.2. 0.22 µm polyester sulfone (PES) was used to determine the effect on the nanoparticle size of THF-made micelles and acetone-made micelles. 0,22 µm was chosen to remove large aggregates and ensure only nanoparticles were analysed, proving a more accurate comparison between the solvents.

The closest value of the targeted size was obtained when the PEG-PLGA micelle was dissolved in acetone and evaporated using an orbital shaker for 24 hours. It was concluded that acetone was not evaporated enough in 6 hours to obtain the targeted micelle size.

4.1.3. Dilusion based stability of PEG-PLGA Micelles

The experiment involved PEG-PLGA micelles created using acetone. The size data were verified through a series of dilutions. These dilutions were made with distilled water, with a dilution factor of 1:2. The aim was to understand the effect of these dilutions on nanoparticle size, which included 1, 1:2, 1:4, 1:8, 1:16, 1:32, 1:64, 1:128, 1:256, 1:512, and 1:1064.

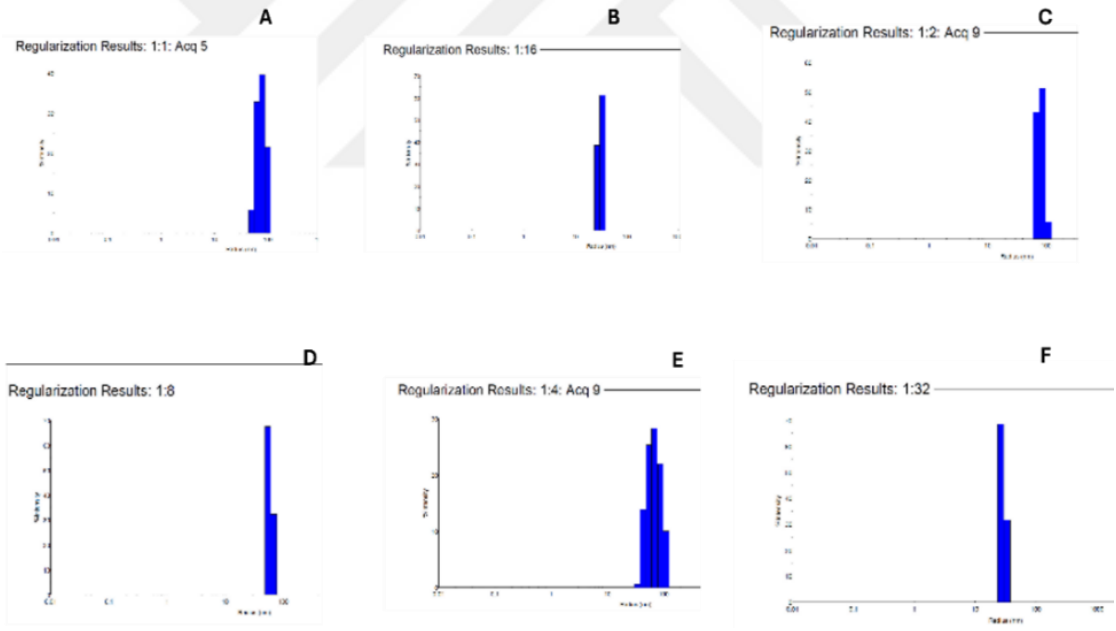

Figure 4.3. Effect of the different dilutions on the NP size. Comparison of nanoparticles prepared in Acetone with PEG-PLGA 1:5 [T/A]: [PP] ratios at various dilutions and filtered using a 0,22 µm Polyester sulfone (PES) filter

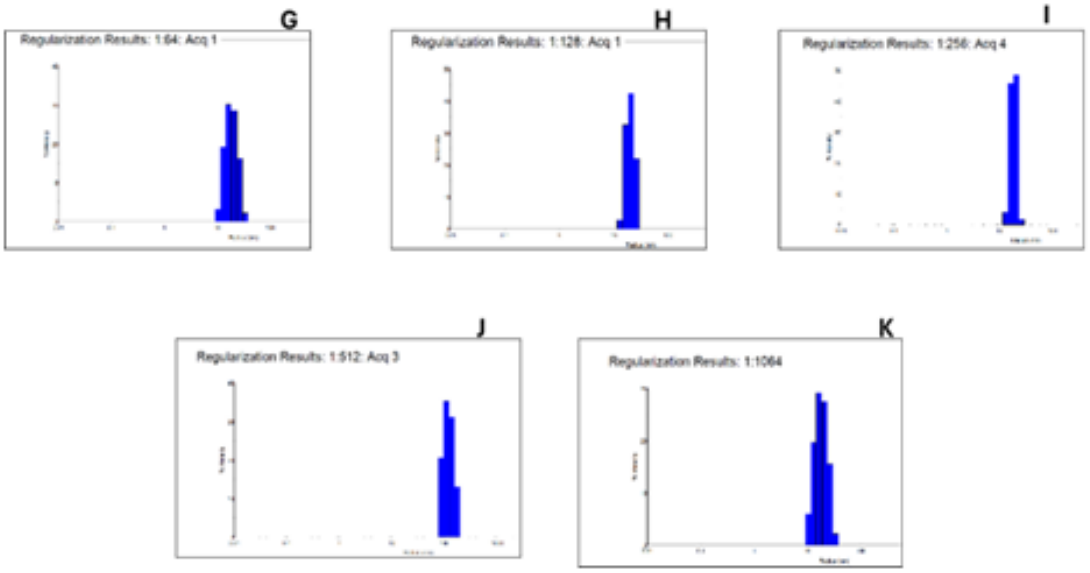

PEG-PLGA Dilutions		
Dilutions	**Diameter (nm)**	**PDI (%)**
1/1	152.92	**20,01**
1/2	160.14	**14,36**
1/4	138.14	**28,88**
1/8	117.10	**11,54**
1/16	61.52	**11,21**
1/32	57.28	**11,49**
1/64	37.66	**27,23**
1/128	40.80	**18,87**
1/256	37.20	**14,16**
1/512	24.60	**22,86**
1/1064	37	**28,35**

Table 4.3. DLS results of PEG-PLGA micelles, diluted in distilled water

As shown in Table 4.3, PEG-PLGA micelles at different dilutions show similar but different characteristics. All the dilutions were filtered with a 0,22 μm Polyester sulfone (PES) filter. Diameter in all the dilutions decreases as dilutions rise. The diameter was relatively high in 1/1 and 1/2 dilutions, as 152.92 nm and 160.14 nm, respectively. The Diameter decreased to 12,30 at 1/512 dilution. This shows smaller dilutions and indicates the formation of more dispersed micelles.

PDI (Polidispersity Index) values show that more homogenised systems were demonstrated at 1/8 and lower dilutions. At 1/8, 1/16, and 1/32 dilutions, PDI values are 11,54%, 11,21%, and 11,49%, respectively, indicating a more monodisperse distribution. But at 1/4 and 1/64 dilutions, PDI values are 28,88% and 27,23%, respectively. These types of high values can mean a more heterogeneous distribution.

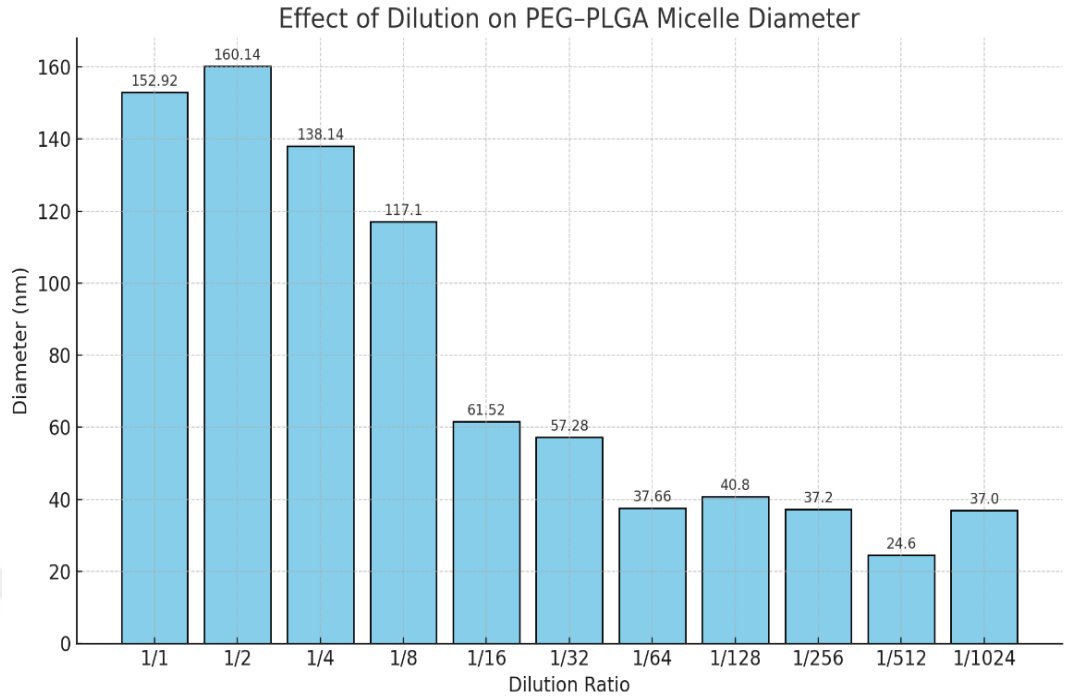

Figure 4.4. The ideal dilution range is between 1/1 and 1/32, where micelles exhibit smaller sizes and improved uniformity. Dilution beyond this range does not consistently enhance Diameter and may result in instability.

The experiment shows that particle sizes were generally smaller after filtration, with low PDI values. This indicates that filtration eliminates larger aggregates, making micelles more homogeneous. This experiment shows that the PEG-PLGA micelles are sensitive to conditions like dilution and filtration, which shows that they extensively affect micelle size and distribution in terms of homogeneity. Reducing micelle size and increasing uniformity can positively influence bioavailability and targeting efficiency, particularly in drug delivery systems.

4.1.4. Zeta Potential Analysis of PEG-PLGA Micelles

Zeta potential measurements showed that blank PEG-PLGA micelles had a surface charge of –21.6 mV, indicating a stable colloidal system. This negative charge is probably due to the polymer's terminal carboxyl groups, which create electrostatic repulsion among particles, thereby improving micelle stability in aqueous environments.

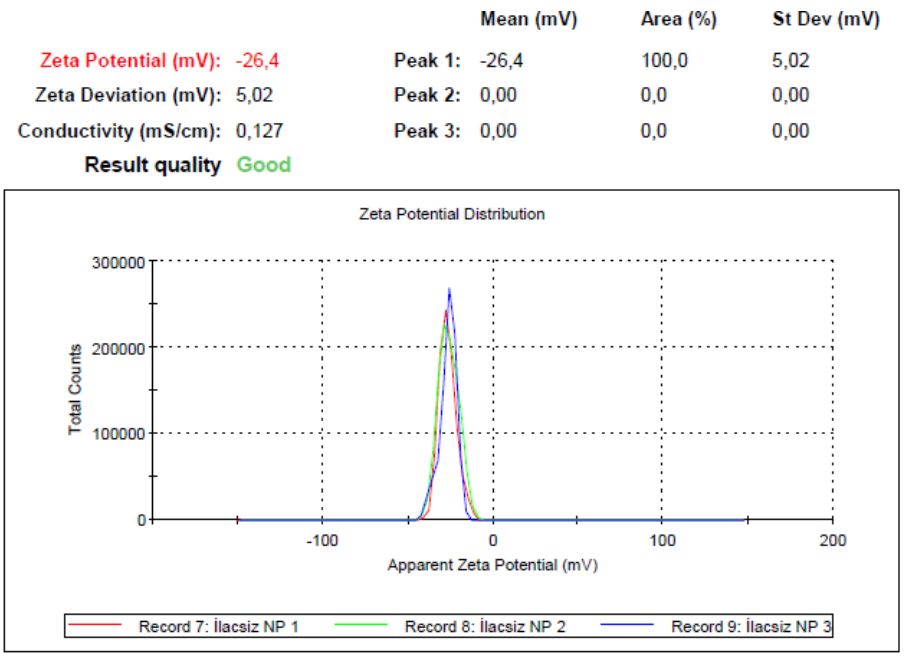

Figure 4.5. Zeta potential of blank PEG-PLGA micelles. The negative surface charge (−21.6 mV) suggests strong colloidal stability from electrostatic repulsion, essential for maintaining nanoparticle dispersion in biological environments.

4.1.5. The Critical Micelle Concentration (CMC) of PEG-PLGA

The critical micelle concentration (CMC) of PEG-PLGA micelles was determined using a fluorescence intensity ratio method based on pyrene emission spectra (ex 338/334 nm). According to the fluorescence ratio vs. log concentration plot, the calculated CMC was approximately $10^{8.15}$ M, indicating high micelle stability and strong self-assembly capability of the PEG-PLGA copolymers in aqueous environments

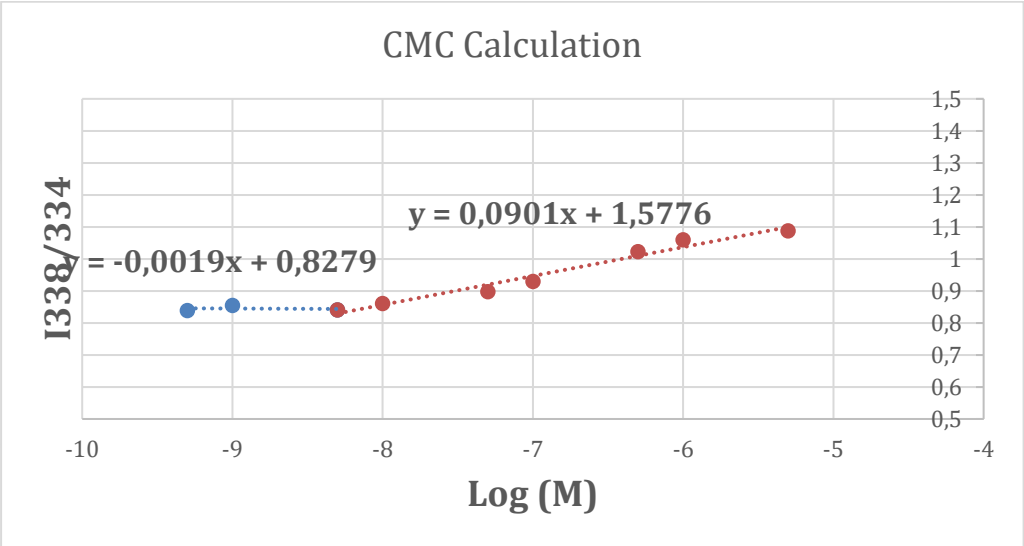

Figure 4.6. The Figure illustrates the fluorescence intensity ratio (I_{388}/I_{334}) of pyrene in relation to the logarithm of PEG-PLGA micelle concentrations. A distinct inflexion point occurs at about logCMC = –8.15, which corresponds to a CMC value of approximately ~$10^{8{\cdot}15}$ M. This inflexion point signals the beginning of micelle formation, as pyrene becomes solubilised in the hydrophobic core of the micelles, leading to a change in its emission profile.

4.2. Preparation and Characterisation of FA-PEG-PLGA Micelles

The DLS analysis revealed distinct differences between FA-loaded PEG–PLGA micelles and non-functionalized PEG–PLGA micelles. The incorporation of folic acid influenced both the hydrodynamic diameter and the polydispersity index (PDI) of the micelles. FA-loaded micelles generally exhibited a slightly increased size compared to blank PEG–PLGA micelles, suggesting that the physical incorporation of folic acid affected the micellar architecture. However, no significant aggregation or instability was observed in either formulation. Repeating the synthesis three times under identical conditions demonstrated consistent results, indicating that evaporation time had a minimal effect on micelle uniformity. These findings suggest that the addition of folic acid, even without chemical conjugation, can subtly alter the micellar structure while maintaining favorable size distribution and colloidal stability—key factors for efficient drug delivery.

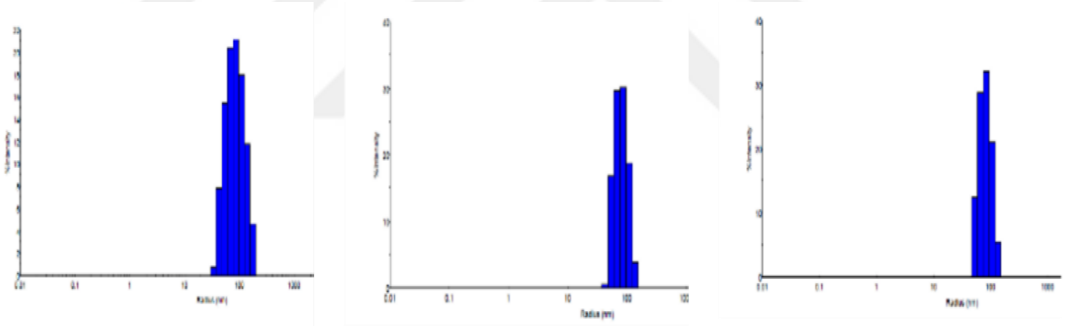

Figure 4.7. Time-dependent changes on the NP size. Comparison of nanoparticles prepared in Acetone with FA- PEG-PLGA 0.5% (w/v) polymer concentration in acetone ratios at different time stamps (A is 2 hours; B is 6 hours; C is 24 hours)

PEG-PLGA Dilutions		
Time (h)	**Diameter (nm)**	**PDI (%)**
2	176,98	29,24
6	163,34	26,11
24	163,56	26,7

Table 4.4. Effect of the Time-dependent changes on the NP size. Comparison of nanoparticles prepared in Acetone with FA- PEG-PLGA 1:5 [A]: [FAPP] ratios at different time stamps (2 hours; 6 hours; 24 hours)

As shown in Table 4.4, FA–PEG–PLGA micelles displayed time-dependent variations in diameter. The micelle diameter decreased over time, suggesting progressive stabilization during solvent evaporation. At 2 and 6 hours, the diameters were relatively high—176.98 nm and 163.34 nm, respectively—while at 24 hours, the diameter slightly reduced to 163.56 nm. This trend indicates that as the evaporation process continues, micelle formation becomes more uniform and stable, resulting in narrower size distribution and improved colloidal properties.

The PDI (Polydispersity Index) values indicate that more homogenised systems are observed as time increases; at 2 hours, the PDI value was 39,34%, while at 6 hours, it dropped to 26,11%. This suggests that micelle uniformity is achieved after 6 hours of evaporation. At 24 hours, the PDI value changed slightly, reaching 26.70%. This result underscores the importance of allowing sufficient time for solvent removal to obtain more homogeneous and stable micelles with folic acid.

This experiment demonstrated that evaporation is a key factor in producing stable micelles. FA-PEG-PLGA micelles are larger than their non-targeted

counterparts. However, since the FA-PEG-PLGA micelles were not filtered, the results remain inconclusive, and 2 hours of evaporation proved insufficient for yielding optimal micelle characteristics.

4.2.1. Preparation and Characterisation of Filtered FA-PEG-PLGA Micelles

Like PEG-PLGA micelles, 0.22 µm polyester sulfone (PES) was used, and a special filter called an Amicon® Ultra centrifugal filter with a 100kDa molecular weight cut off was used. This double filtration process allowed for the removal of large aggregates and unencapsulated small molecules like free folic acid, and to determine the effect on the nanoparticle size of FA-PEG-PLGA micelles. Amicon® ultrafiltration allowed for removing large aggregates and unencapsulated small molecules, including free folic acid, resulting in micelles with reduced size and polydispersity index (PDI)

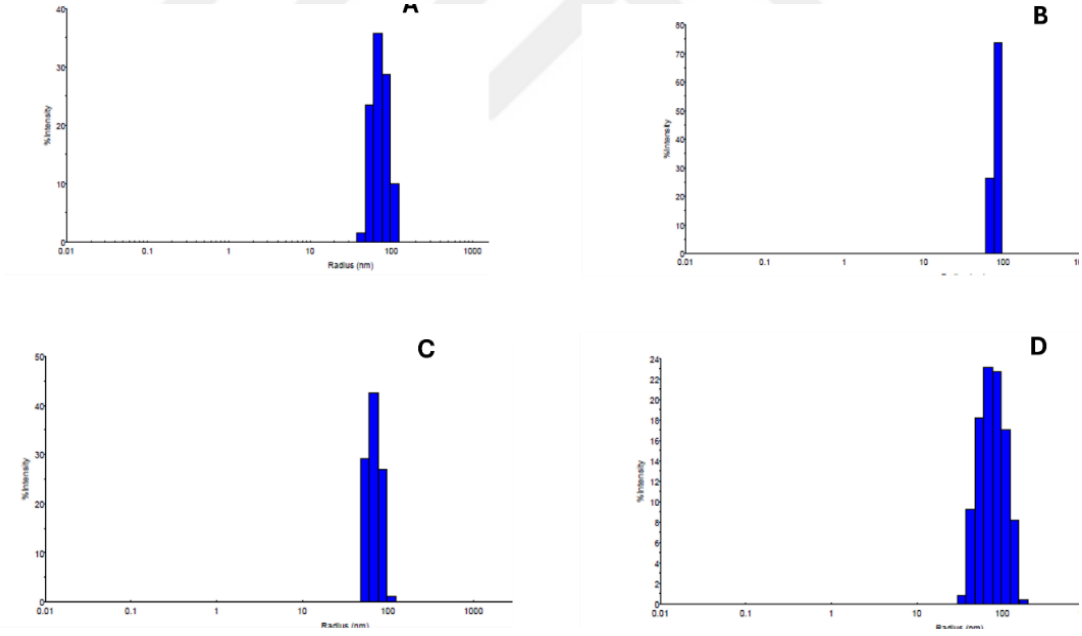

Figure 4.8. Effect of the Time and filter-dependent changes on the NP size via DLS. Comparison of nanoparticles prepared in Acetone with FA- PEG-PLGA 1:5 [A]: [FAPP] ratios at different time stamps (A is 6 hours; B is 24 hours) with 0.22µm polyester sulfone (PES) and an Amicon® Ultra centrifugal filter was used (C is non-filtered; D is filtered).

FA-PEG-PLGA 6 hours		
W/Filtration	**Diameter (nm)**	**PDI (%)**
Without Filtration	163,96	9,85
With Filtration	161,4	34,97

FA-PEG-PLGA 24 hours		
W/Filtration	**Diameter (nm)**	**PDI (%)**
Without Filtration	147,98	23,99
With Filtration	139	18,71

Table 4.5. Effect of the Time and filter-dependent changes on the NP size via DLS. Comparison of nanoparticles prepared in Acetone with FA- PEG-PLGA 1:5 [A]: [FAPP] ratios at different time stamps (6 hours; 24 hours) with 0.22 μm polyester sulfone (PES) and an Amicon® Ultra centrifugal filter.

As shown in the table, filtration is essential on both size and polydispersity index.

At the 6th hour, the unfiltered micelles had a Diameter of 163,96nm and a low PDI of 9.85%, indicating a moderately uniform size distribution. But, after filtration, the Diameter changes slightly, decreasing to 161,40nm, while the PDI rises to 34,97%. This can mean that filtration could have disrupted the micelle population.

At the 24th hour, the effects of filtration were more aligned with expectations. The unfiltered micelles had a larger Diameter of 147,98nm and a higher PDI of 23.99%, meaning greater size variation. After filtration, the micelles became smaller by 139,00nm and more uniform by 18,71%. This indicates that with longer evaporation times, filtration removes aggregates and unencapsulated components more effectively, resulting in a more refined nanoparticle population. “FA-PEG-PLGA micelles show larger particle sizes and slightly higher PDI values than PEG-PLGA micelles.”

4.2.2. Zeta Potential Analysis of FA-PEG-PLGA Micelles

Zeta potential measurements showed that unmodified FA-PEG-PLGA micelles had a surface charge of –29.1 mV, indicating enhanced colloidal stability compared to non-functionalized PEG-PLGA micelles. The increased negative potential is likely due to the folic acid moieties on the micelles' surface, which may provide additional ionisable groups, thus increasing electrostatic repulsion and facilitating dispersion in aqueous environments.

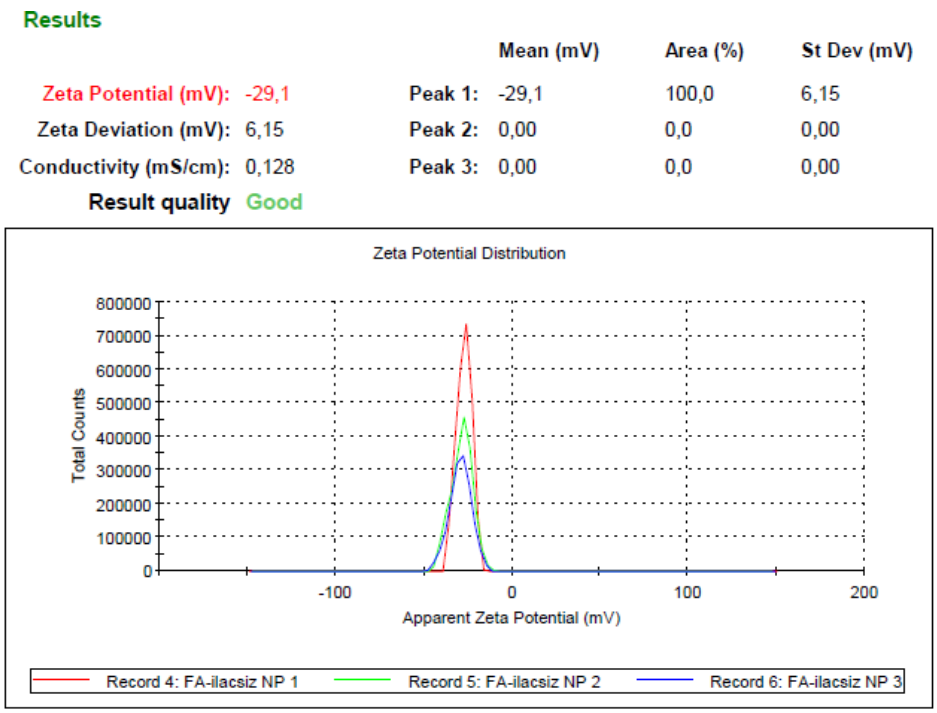

Figure 4.9. Zeta potential of blank FA-PEG-PLGA micelles. The surface charge was measured as −29.1 mV, indicating a moderately negative surface potential. This value is likely influenced by the folic acid present on the micelle surface, which contributes to stability and potential targeting capability in biological environments.

4.3. Encapsulation of Hydrophobic Compounds in PEG-PLGA Micelles

To evaluate the micelles' ability to encapsulate hydrophobic molecules, a model dye—Nile Red—was incorporated into PEG–PLGA micelles. This process helped to simulate drug loading and visualize micellar behavior through fluorescence.

4.3.1. Encapsulation of Nile Red in PEG-PLGA Micelle

Nile Red served as a model hydrophobic compound to understand the encapsulation capability and stability of PEG-PLGA micelles. As a fluorescent dye with lipophilic characteristics, Nile Red is excellent for visualising drug distribution and tracking release kinetics in vitro. Incorporating such molecules into micelles enhances their solubility and offers valuable insights into the behaviour of drug-loaded systems in physiological conditions.

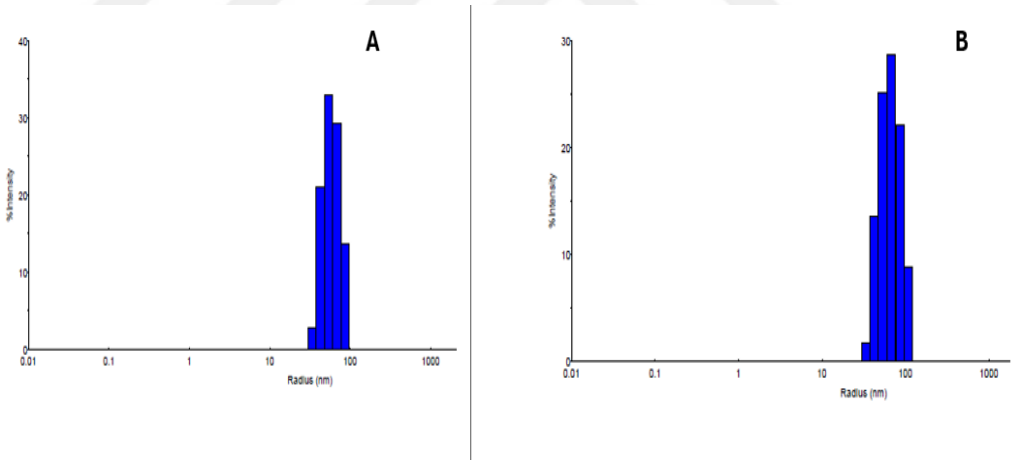

Figure 4.10. Effect of the targeted and non-targeted micelles on Nile red nanoparticle. Comparison of nanoparticles prepared in Acetone with FA- PEG-PLGA and PEG-PLGA 1:5 [A]: [FAPP/PP] ratios at 24 hours without 0.22 μm polyester sulfone (PES) and an Amicon® Ultra centrifugal filter.

Without Filtration	Diameter (nm)	PDI (%)
Nile Red PEG-PLGA	135,88	28,91
Nile Red FA-PEG-PLGA	119,34	24,56

Table 4.6. Effect of the targeted and non-targeted micelles on Nile red nanoparticle. Comparison of nanoparticles prepared in Acetone with FA- PEG-PLGA and PEG-PLGA 1:5 [A]: [FAPP/PP] ratios at 24 hours without 0.22 μm polyester sulfone (PES) and an Amicon® Ultra centrifugal filter

The encapsulation of Nile Red into FA-PEG-PLGA and PEG-PLGA micelles allowed for a comparative estimation of targeting and non-targeting systems. Data showed that the FA-PEG-PLGA micelles showed a smaller particle size, 119,34, and a lower PDI, 24,56, compared to PEG-PLGA.

These findings imply that folic acid may enhance micelle density or support a more uniform assembly during encapsulation. Notably, this contrasts with unloaded micelles, where FA-PEG-PLGA appeared larger. This change might suggest that the interaction between Nile Red and the polymer structure aids in stabilising the targeted micelles.

However, as both systems were unfiltered, the results represent the micelles' natural assembly behaviour and should be considered preliminary. Additional filtration and stability studies are necessary to establish if folic acid consistently aids in reducing size and enhancing homogeneity in drug-loaded formulations.

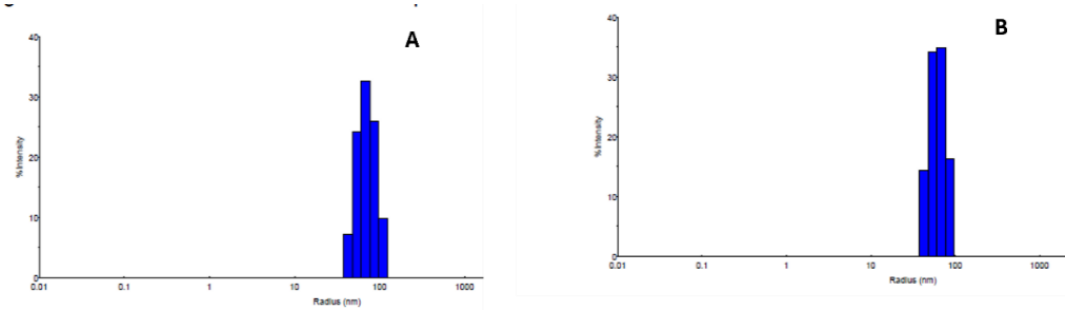

Figure 4.11. Effect of filtration on the targeted and non-targeted micelles on Nile red nanoparticle. Comparison of nanoparticles prepared in Acetone with FA-PEG-PLGA and PEG-PLGA 1:5 [A]: [FAPP/PP] ratios at 24 hours with 0.22 μm polyester sulfone (PES) and an Amicon® Ultra centrifugal filter used

With Filtration	Diameter (nm)	PDI (%)
Nile Red PEG-PLGA	125,32	22,01
Nile Red FA-PEG-PLGA	143,56	25,85

Table 4.7. Effect of the filtration on targeted and non-targeted micelles of Nile red nanoparticle. Comparison of nanoparticles prepared in Acetone with FA- PEG-PLGA and PEG-PLGA 1:5 [A]: [FAPP/PP] ratios at 24 hours with 0.22 μm polyester sulfone (PES) and an Amicon® Ultra centrifugal filter

After filtration, the FA-PEG-PLGA and PEG-PLGA micelles demonstrated decreased particle size and PDI compared to those that were not filtered. However, a notable difference continued between the targeted and non-targeted systems.

The filtered FA-PEG-PLGA micelles presented a Diameter of 143,56 nm and a PDI of 25.85%, while the filtered PEG-PLGA micelles were smaller, with a Diameter of 125,32 nm and a slightly reduced PDI of 22.01%. These findings imply that including folic acid in the formulation may marginally elevate particle size and heterogeneity, even post-filtration.

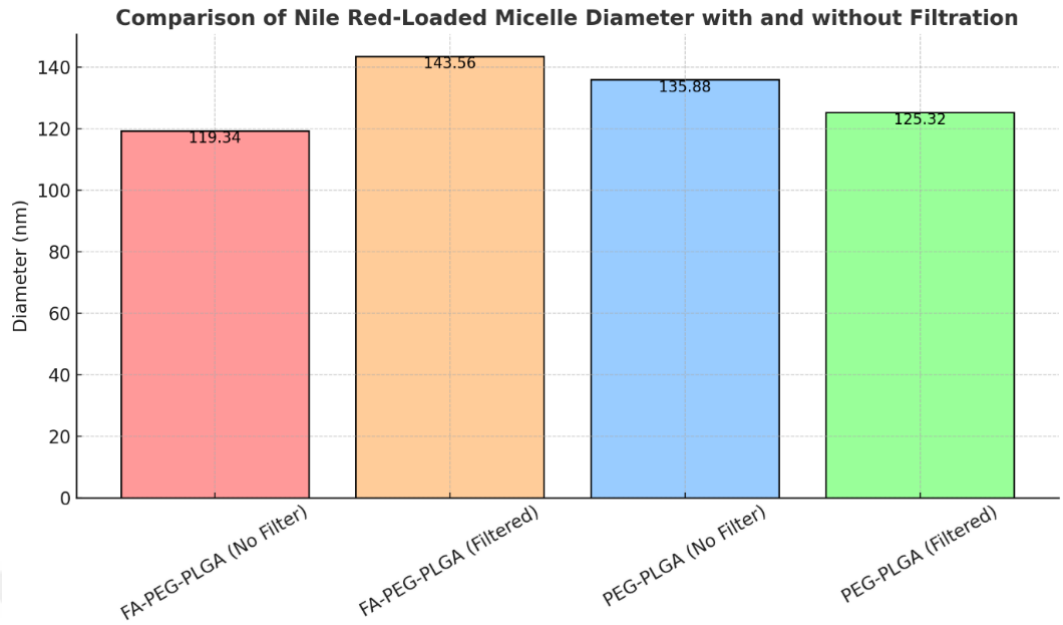

Figure 4.12. This Figure compares the hydrodynamic Diameter of Nile Red-loaded FA-PEG-PLGA and PEG-PLGA micelles, both filtered and unfiltered. Initially, FA-PEG-PLGA micelles had a smaller Diameter when unfiltered, but their size increased after filtration. Conversely, PEG-PLGA micelles exhibited a decrease in size following filtration.

This effect could be attributed to surface interactions between folic acid and polymer chains or potential steric hindrance impacting self-assembly. However, filtration was crucial in eliminating larger aggregates and refining the particle size distribution in both formulations.

4.4. Preparation and Evaluation of Drug-Loaded PEG-PLGA Micelles

Active compounds were encapsulated in non-targeted micelles at different concentrations to explore the drug loading capacity and structural response of PEG-PLGA micelles. The encapsulation process began with the PEG-PLGA system alone, without any targeting ligand. Each compound was evaluated at three different drug-to-polymer ratios: 5%, 10%, and 20% (w/w).

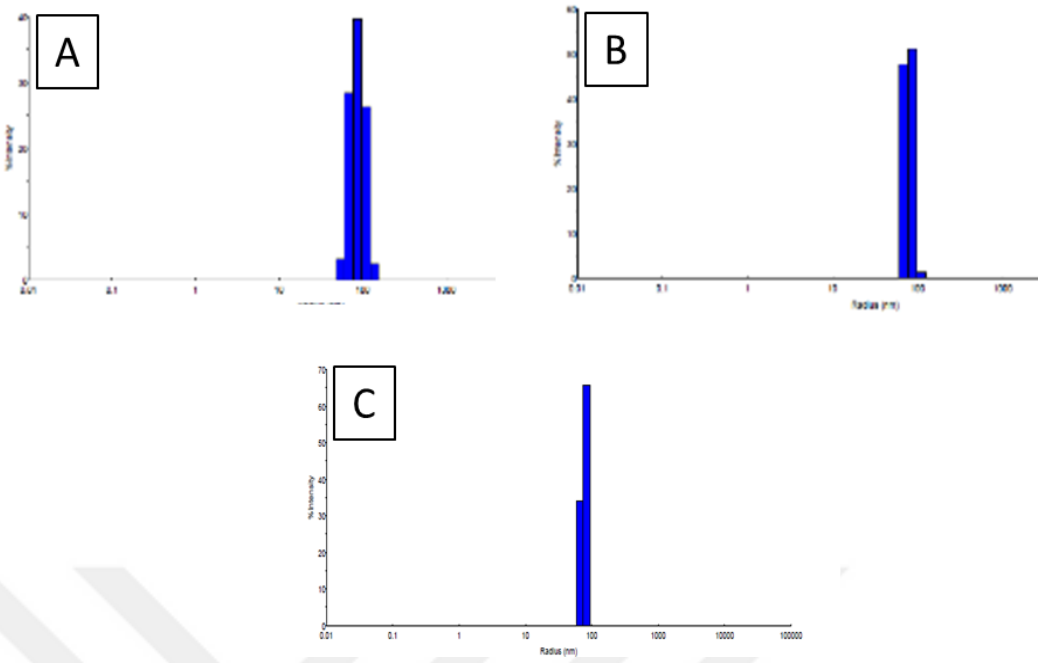

Figure 4.13. Effect of different drug ratios: A is 5%, B is 10%, and C is 20% (w/w) on non-targeted micelles. Comparison of nanoparticles prepared in Acetone with PEG-PLGA 1:5 [A]: PP] ratios at 24 hours with 0.22 μm polyester sulfone (PES) and an Amicon® Ultra centrifugal filter.

This experiment shows how increases in drug concentration affect micelle size and uniformity while exploring the relationship between drug loading percentage and micellar stability. This section emphasises the physical characterisation of these drug-loaded micelles, evaluated by their hydrodynamic diameter and polydispersity index (PDI), which will form a basis for future comparisons with folic acid-modified (FA-PEG-PLGA) targeting systems.

3 AB-PEG-PLGA		
Drug Ratios (%)	**Diameter (nm)**	**PDI (%)**
5	175,62	20,96
10	156,4	12,52
20	132,52	17,28

Table 4.8. Effect of different drug ratios: 5%, 10%, and 20% (w/w) on non-targeted micelles. Comparison of nanoparticles prepared in Acetone with PEG-PLGA 1:5 [A]: [PP] ratios at 24 hours with 0.22 μm polyester sulfone (PES) and an Amicon® Ultra centrifugal filter.

The impact of drug loading concentration on micelle size and homogeneity was assessed using PEG-PLGA micelles loaded with one of three same active compounds. At a 5% drug-to-polymer ratio, the micelle Diameter was 175,62 nm, accompanied by a polydispersity index (PDI) of 20.96%. When the concentration increased to 10%, the micelle Diameter decreased to 156,40 nm, and the PDI improved to 12.52%, suggesting a more uniform distribution. However, at a 20% loading, a dramatic reduction in micelle size to 132,52 nm was observed, along with a significant increase in PDI to 39.39%, indicating instability and the potential for aggregation.

4.6. Zeta Potential Analysis of 3 AB Loaded PEG-PLGA Micelles

Zeta potential measurements indicated that 3AB-loaded PEG-PLGA micelles displayed a surface charge of –0.977 mV at 5% drug loading, 0.0319 mV at 10%, and –0.356 mV at 20%. These results show a significant reduction in surface charge compared to blank PEG-PLGA micelles (–21.6 mV), highlighting that drug encapsulation has an important impact on micellar surface properties.

The nearly neutral zeta potential observed at all drug-loading ratios implies a potential decrease in colloidal stability due to diminished electrostatic repulsion. This phenomenon may be linked to the masking of functional groups on the surface by the encapsulated 3AB molecules or possible structural rearrangements in the micelles upon drug loading. Nonetheless, the micelles preserved a stable dispersion without visible aggregation, indicating that steric stabilisation from the PEG might still provide a protective effect despite the lack of strong electrostatic repulsion.

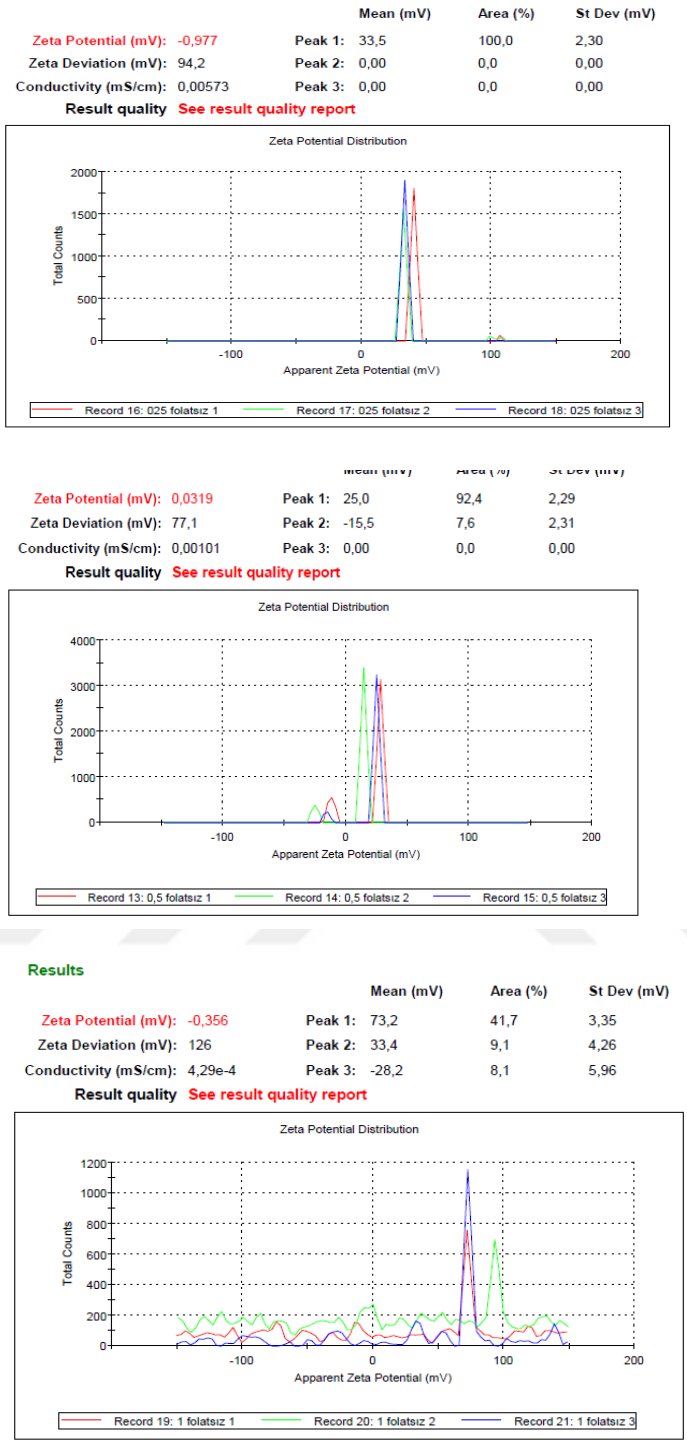

Figure 4.14. Zeta potential measurements indicated that 3AB-loaded PEG-PLGA micelles displayed a surface charge of –0.977 mV at 5% drug loading, 0.0319 mV at 10%, and –0.356 mV at 20%. This value is likely influenced by the drug on the micelle surface, contributing to stability and potential targeting capability in biological environments.

4.5. Preparation and Evaluation of Drug-Loaded FA-PEG-PLGA Micelles

To evaluate the influence of folic acid targeting on drug-loaded micellar systems, the same three active compounds were encapsulated into FA-PEG-PLGA micelles using the same drug-to-polymer ratios (5%, 10%, and 20%). The objective was to determine how folic acid's presence impacts micelle size, uniformity, and stability at increasing drug concentrations.

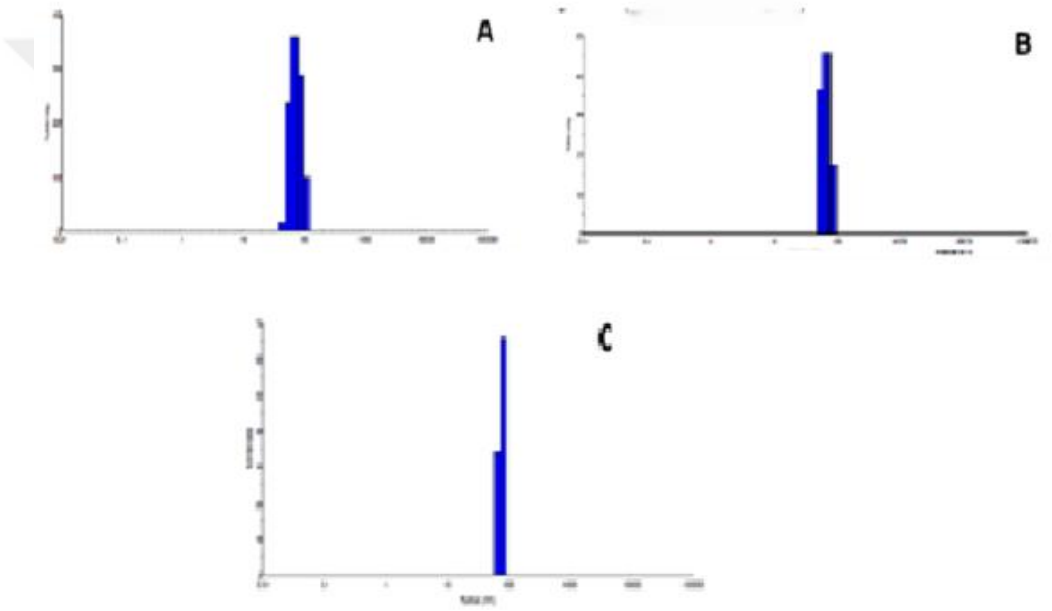

Figure 4.15. Effect of different drug ratios: A 5%, B 10%, and C 20% (w/w) on targeted micelles. Comparison of nanoparticles prepared in Acetone with FA- PEG-PLGA 1:5 [A]: [FAPP] ratios at 24 hours with 0.22 μm polyester sulfone (PES) and an Amicon® Ultra centrifugal filter

Like the non-targeted systems, physical characterisation was performed by measuring hydrodynamic diameter and polydispersity index (PDI). The results from the FA-modified micelles were compared to those of the PEG-PLGA micelles to deepen our understanding of folic acid's role in preserving micelle integrity at varying loading conditions.

3 AB-FA-PEG-PLGA		
Drug Ratios (%)	**Diameter (nm)**	**PDI(%)**
5	147,98	23,39
10	132,52	17,28

Samples	**Drug Encapsulation Efficiency (%)**	**Drug Feed Amount (µg)**	**Drug Obtained Amount (µg)**
	5% 10% 20%	5% 10% 20%	5% 10% 20%
PLGA-PEG Micelles	94.4 54.7 35.9	215,2 311,2 319,5	250 500 1000
FA PLGA-PEG Micelles	86.1 62.2 32	236,1 273,6 359,2	250 500 1000

Table 4.9. Drug encapsulation efficiency (EE%) decreased as the initial drug-to-polymer ratio increased. The highest EE% was observed at 5% loading for both non-targeted (94.4%) and FA-targeted (86.1%) micelles. The significant decline at 20% loading suggests reaching the maximum capacity of the micellar core.

The impact of drug loading on FA-PEG-PLGA micelles was measured at drug-to-polymer ratios of 5%, 10%, and 20%. At a 5% loading, the micelle diameter measured 147.98 nm, accompanied by a polydispersity index (PDI) of 23.39%.

Increasing the loading to 10% led to a reduced diameter of 132.52 nm and an improved PDI of 17.28%, indicating a more uniform micelle population. However, at a 20% loading, the diameter increased to 153.86 nm, while the PDI significantly increased to 42.02%, suggesting notable heterogeneity and potential instability at higher drug concentrations.

4.7. Zeta Potential Analysis of 3 AB Loaded FA-PEG-PLGA Micelles

Zeta potential analysis of FA-PEG-PLGA micelles loaded with 3AB showed surface charge values of –0.374 mV at 5% drug loading, 0.0856 mV at 10%, and –0.0359 mV at 20%. When compared to the blank FA-PEG-PLGA micelles showing–29.1 mV, these results indicate a notable decrease in negative surface potential due to drug encapsulation.

The nearly neutral zeta potential across all concentrations suggests that the presence of 3AB molecules may be affecting the micellar surface environment, potentially by shielding charged functional groups or modifying micelle packing. Even with reduced electrostatic repulsion, no observable aggregation was noted, implying that steric stabilization from the PEG chains is effective in preserving micelle dispersion.

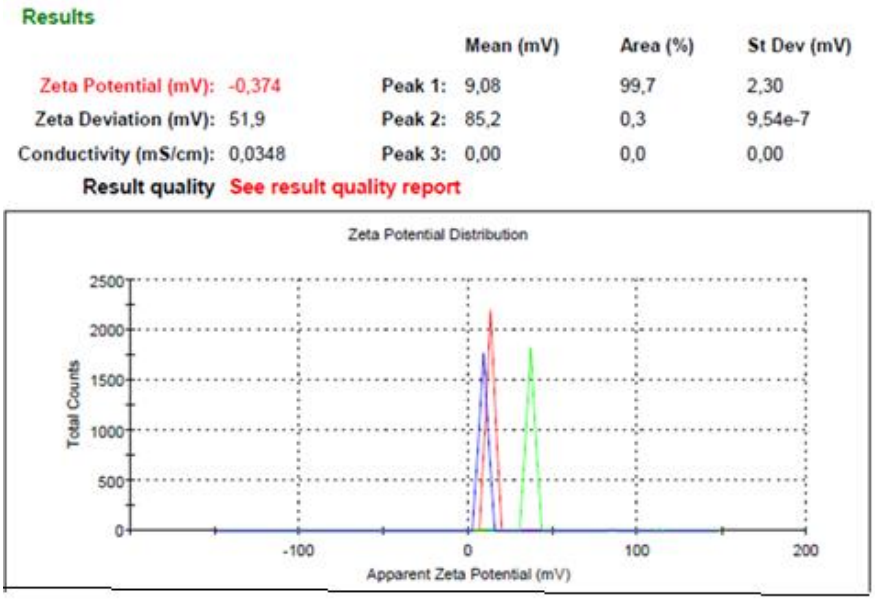

Figure 4.15. Zeta potential analysis of FA-PEG-PLGA micelles loaded with 3AB at 5% drug loading showed a surface charge value of –0.374 mV. This value is likely influenced by the presence of the drug on the micelle surface, contributing to stability and potential targeting capability in biological environments.

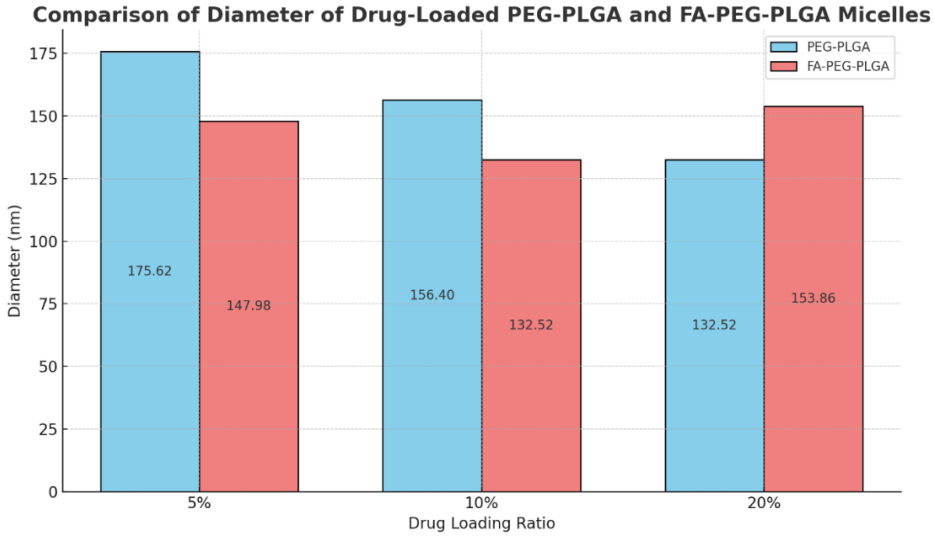

Figure 4.16. Comparison of the hydrodynamic Diameter of PEG-PLGA and FA-PEG-PLGA micelles at various drug loading ratios (5%, 10%, and 20%). FA-modified micelles showed a lower Diameter at 5% and 10%, while a higher Diameter was observed at 20%, indicating structural variation under high drug loading.

4.8. Evaluation of Drug-Encapsulation Efficiency

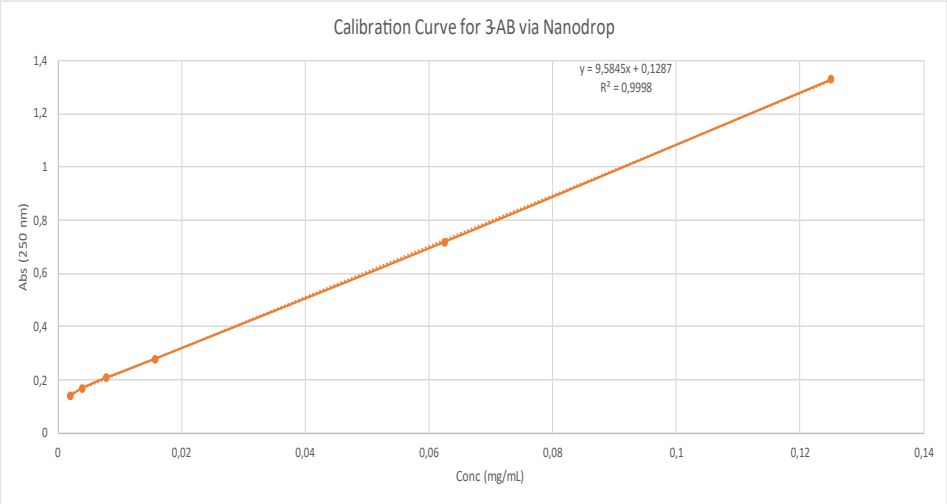

Figure 4.17. Shows the calibration curve for 3-AB, obtained through UV-Vis spectrophotometry at a wavelength of 250 nm. The linear regression equation is y = 9.5845x + 0.1287, exhibiting a correlation coefficient (R^2) of 0.9998, demonstrating good linearity between absorbance and concentration.

4.9. Drug Release Profiles of 3-AB-Loaded Micelles under Different pH Conditions

As shown in the graph, both 5% and 10% drug-loaded micelles exhibited a faster and more extensive drug release at pH 5.5, mimicking the acidic tumor microenvironment, compared to the physiological pH 7.4**.**

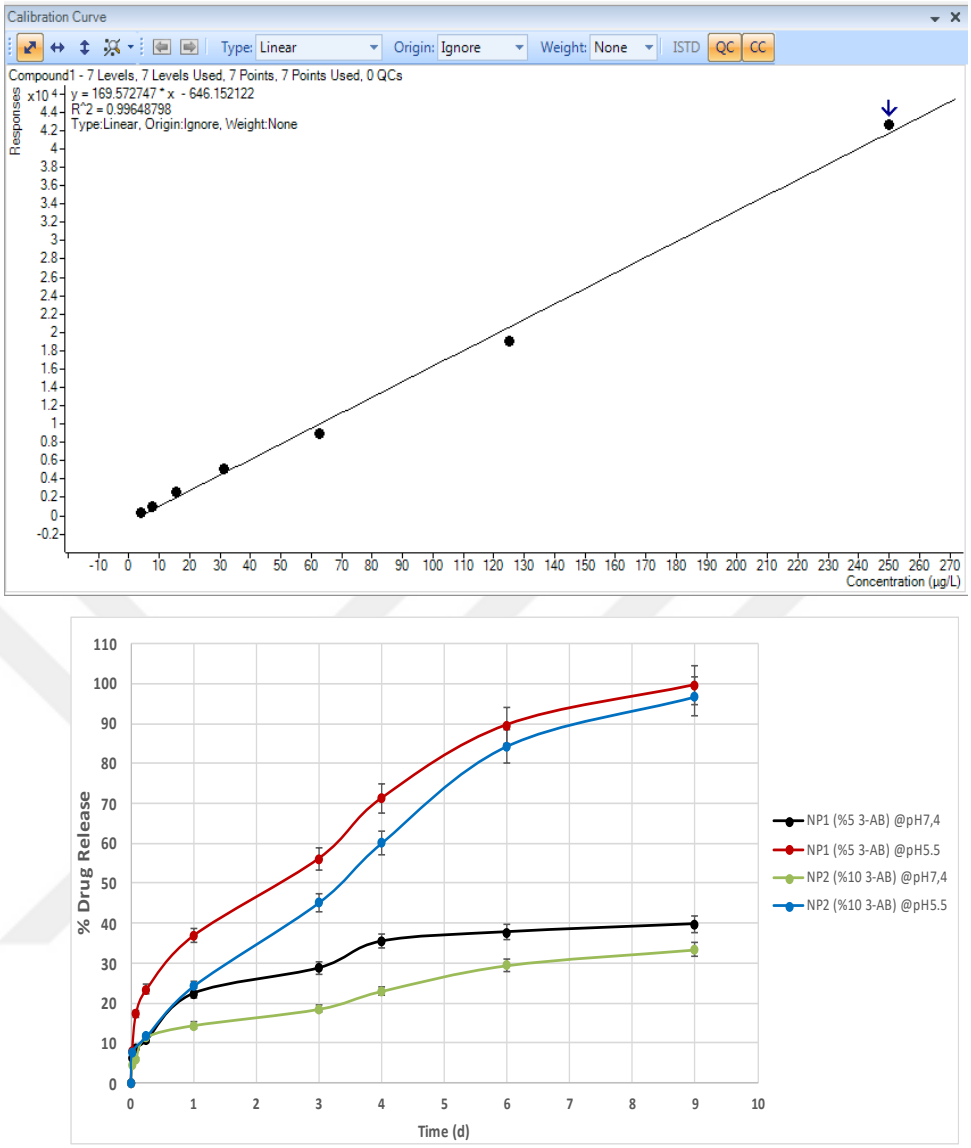

Figure 4.18. The release behavior of 3-AB from PEG–PLGA micelles was evaluated using the dialysis method in phosphate-buffered saline (PBS, pH 7.4) and acetate buffer (pH 5.5) at 37°C for 9 days. Samples were collected at predetermined time intervals and analyzed by LC–MS/MS.

Notably, **NP1 (5% 3-AB)** demonstrated the highest release (~99%) at pH 5.5, indicating a pH-sensitive release profile that could enhance drug accumulation in acidic tumor tissues.

4.10. Cytotoxicity Assessment by CCK-8 Assay

The CCK-8 assay showed that blank PEG-PLGA and FA-PEG-PLGA micelles exhibited low cytotoxicity towards SKOV-3 cells, indicating their biocompatibility. On the contrary, free 3AB notably decreased cell viability dose-dependently, demonstrating its intrinsic cytotoxic effect. These results emphasise the safety profile of the micellar carriers and serve as a reference point for assessing drug-loaded formulations.

Additionally**,** the CCK-8 assay was also performed on the L929 fibroblast cell line to evaluate the cytotoxicity of the formulations on non-cancerous cells. FA-PEG-PLGA micelles showed negligible toxicity on L929 cells, similar to their effect on SKOV-3 cells. Notably, free 3AB also exhibited dose-dependent cytotoxicity on L929 cells, although to a lesser extent compared to SKOV-3. These results support the notion that the micellar formulation reduces off-target toxicity and improves the safety of 3AB delivery in healthy tissues.

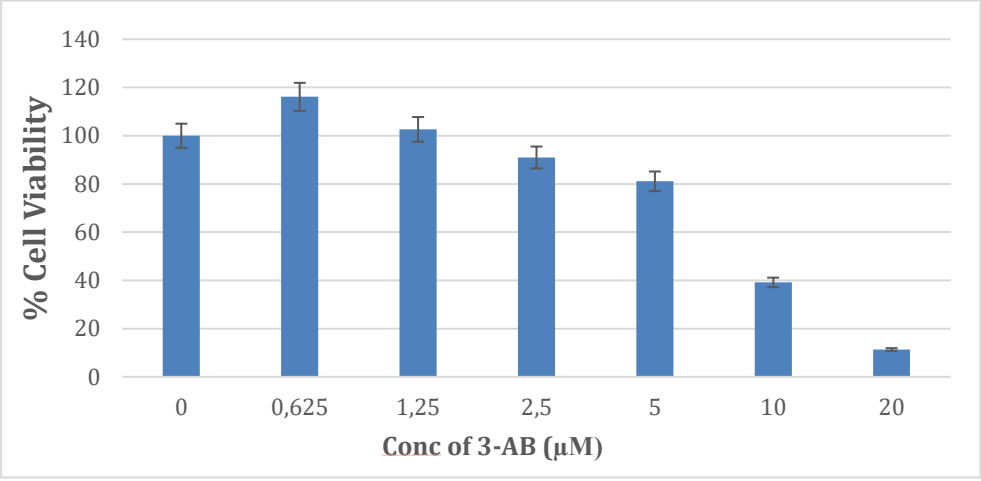

Figure 4.19. Effect of free 3-AB on SKOV-3 cell viability at various concentrations (0–20 µM).

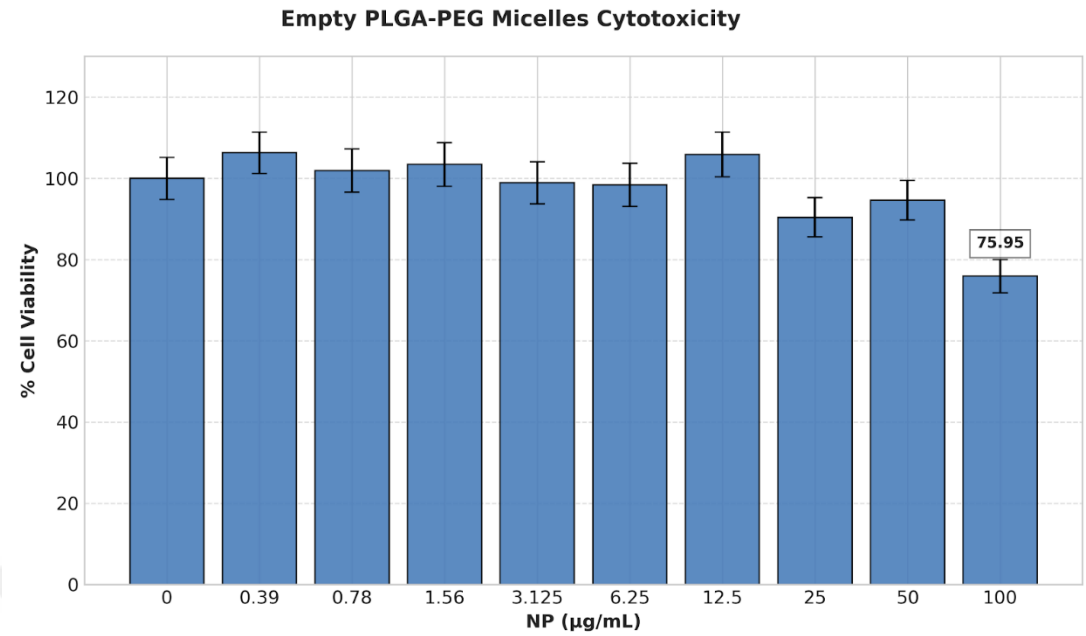

Figure 4.20. The in vitro cytotoxicity of empty PLGA–PEG micelles was evaluated across a concentration range of 10 to 100 µg/mL on SKOV-3 cells to ensure the carrier's biocompatibility

SKOV-3 Cells were treated with increasing concentrations of 3-aminobenzamide (3-AB) for 24 hours, and cell viability was assessed using the CCK-8 assay. Data are presented as mean ± standard deviation (n=3). Higher concentrations of 3-AB, particularly 10 µM and 20 µM, resulted in significant cytotoxicity compared to the treated control group.

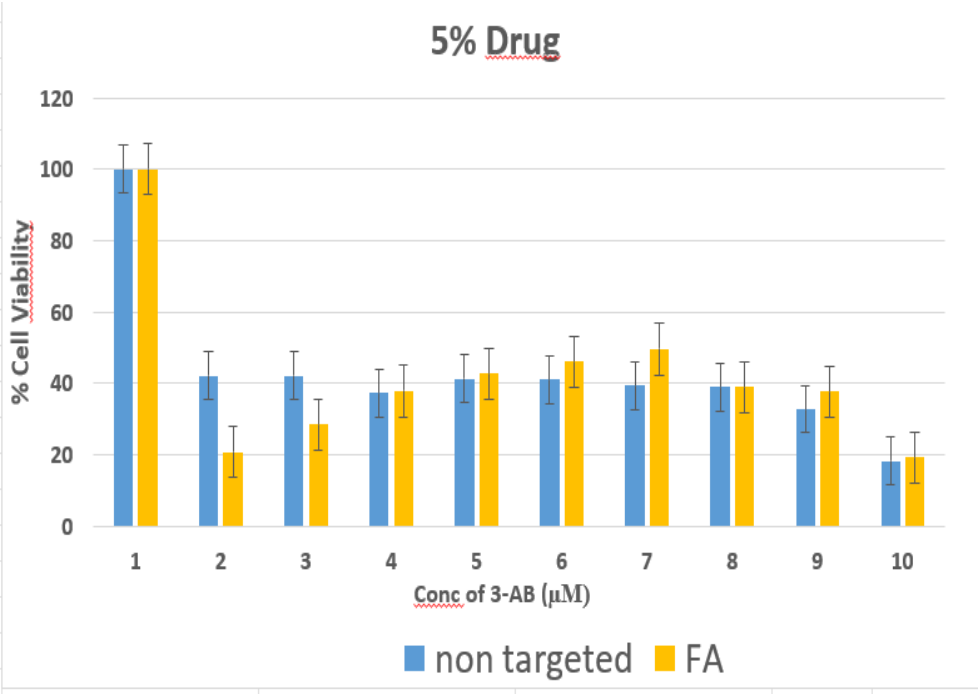

Figure 4.21. Effect of 5% 3-AB loaded and **4% (w/w) FA-modified** PEG–PLGA micelles on SKOV-3 cell viability at various concentrations (0–20 µM).

SKOV-3 Cells were treated with increasing concentrations of 3-aminobenzamide (3-AB) for 24 hours, and cell viability was assessed using the CCK-8 assay. Data are presented as mean ± standard deviation (n=3). Higher concentrations of 3-AB, particularly 20 µM, resulted in significant cytotoxicity compared to the treated control group

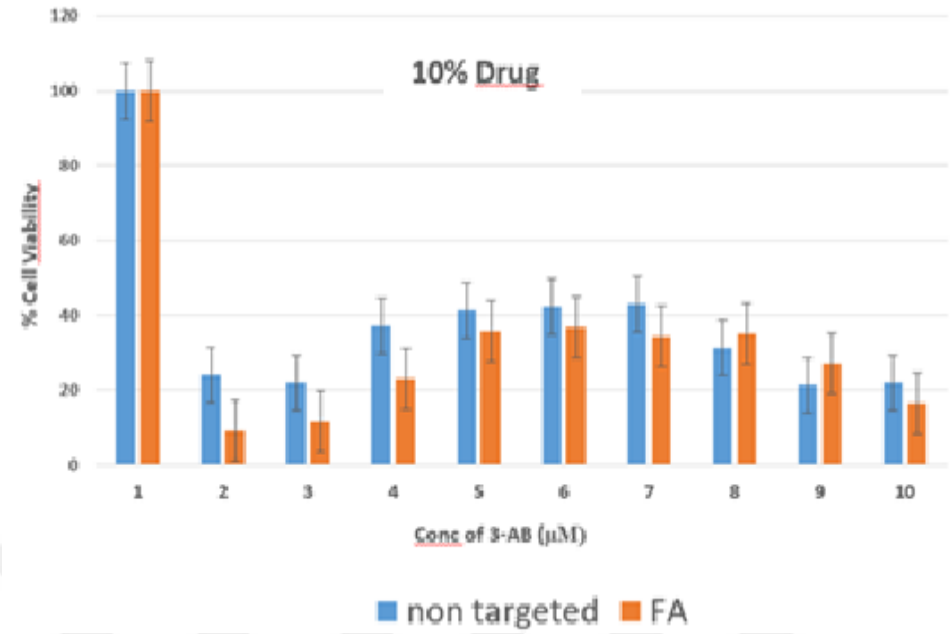

Figure 4.22. Effect of 10% 3-AB loaded and 4% (w/w) FA-modified PEG–PLGA micelles on SKOV-3 cell viability at various concentrations (0–20 µM).

SKOV-3 Cells were treated with increasing concentrations of 3-aminobenzamide (3-AB) for 24 hours, and cell viability was assessed using the CCK-8 assay. Data are presented as mean ± standard deviation (n=3). Higher concentrations of 3-AB, particularly 20 µM, resulted in significant cytotoxicity compared to the treated control group.

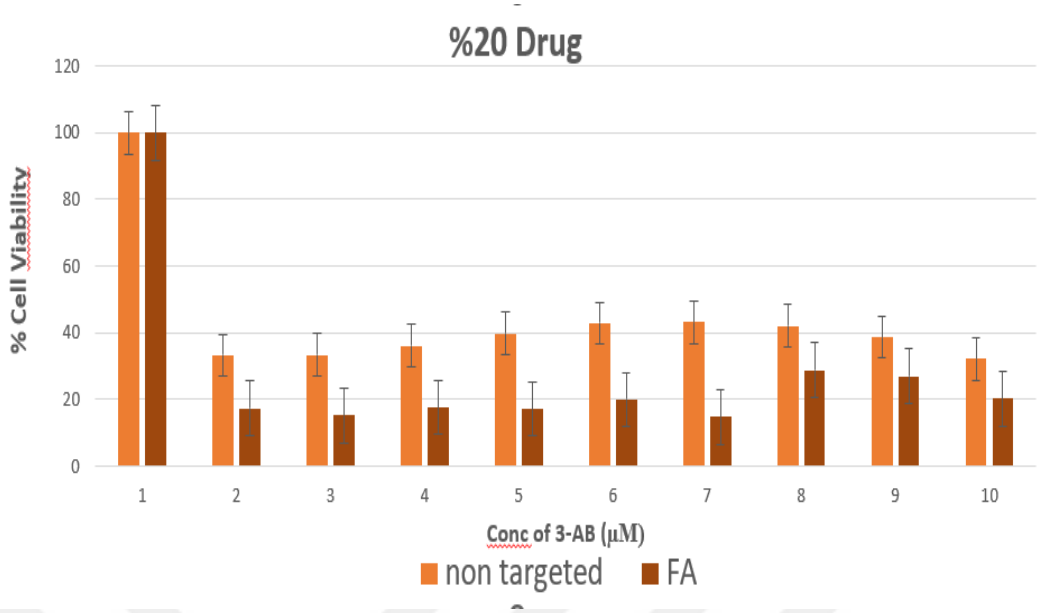

Figure 4.23. Effect of 20% 3-AB loaded and 4% (w/w) FA-modified PEG–PLGA micelles on SKOV-3 cell viability at various concentrations (0–20 µM).

SKOV-3 Cells were treated with increasing concentrations of 3-aminobenzamide (3-AB) for 24 hours, and cell viability was assessed using the CCK-8 assay. Data are presented as mean ± standard deviation (n=3). All concentrations of 3-AB resulted in significant cytotoxicity compared to the treated control group.

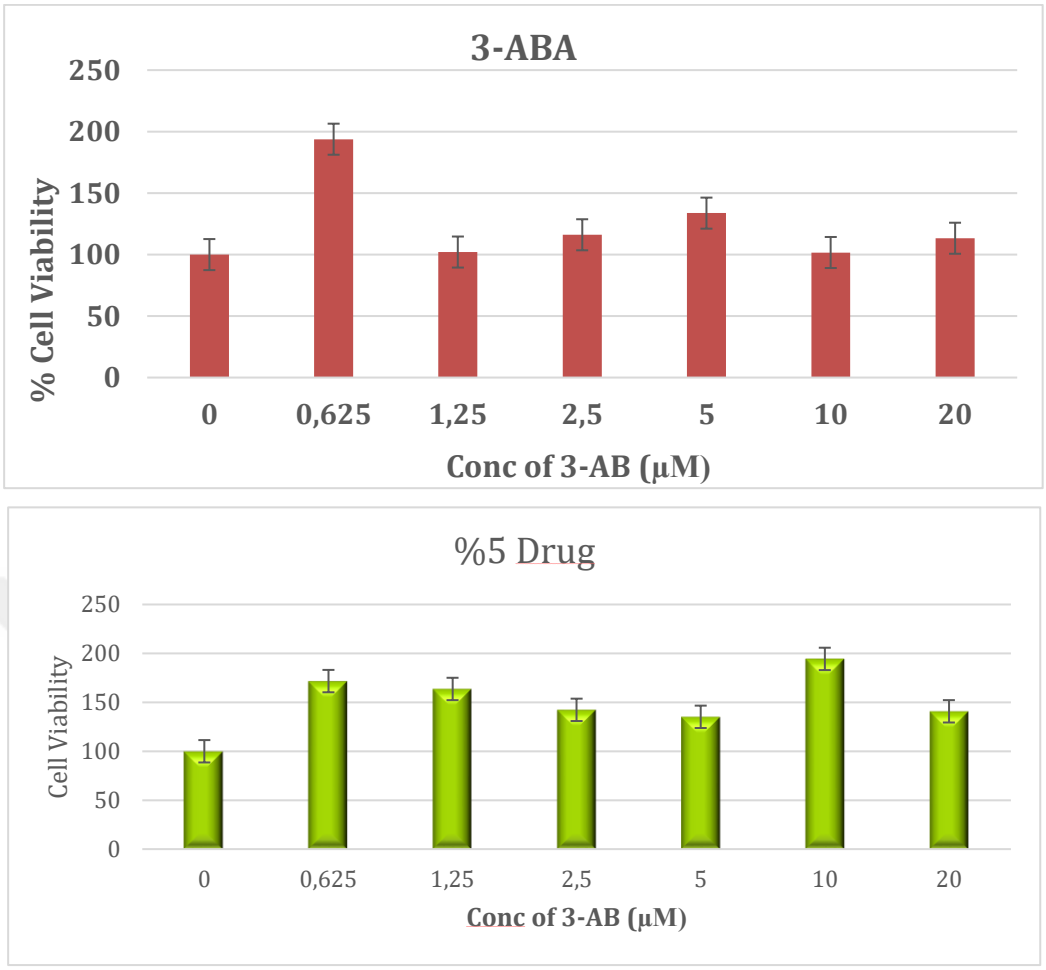

Figure 4.24. Evaluation of cytotoxicity of 10% and free 3ABA loaded PEG–PLGA against L929 cells.

L929 fibroblast cells were incubated with blank micellar formulations at different polymer concentrations ranging from 0.078 µM to 20 µM for 24 hours. Cell viability was measured using the CCK-8 assay. Both 5% and 10% drug loaded PEG–PLGA micelles exhibited minimal cytotoxicity across all concentrations, indicating the biocompatibility of the carrier system. Data are expressed as mean ± SD (n=3).

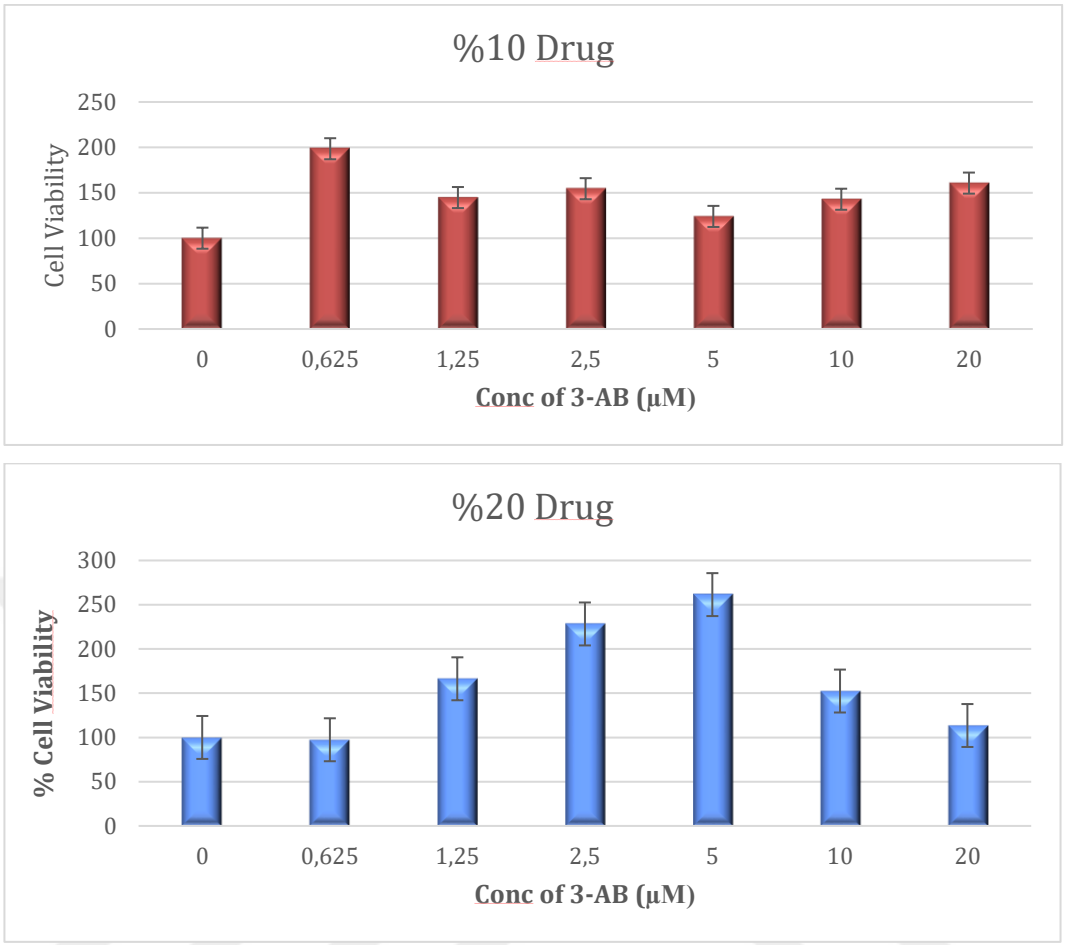

Figure 4.25. Evaluation of cytotoxicity of 20% drug loaded PEG–PLGA and 5% drug loaded on L929 cells.

L929 fibroblast cells were incubated with blank micellar formulations at different polymer concentrations ranging from 0.078 µM to 20 µM for 24 hours. Cell viability was measured using the CCK-8 assay. Both drug-loaded PEG–PLGA micelles and free 3 ABA exhibited minimal cytotoxicity across all concentrations, indicating the biocompatibility of the carrier system. Data are expressed as mean ± SD (n=3).

4.9. CELL INTERNALISATION STUDIES

Fluorescence microscopy was done to assess the cellular uptake of Nile Red in SKOV-3 cells across different treatment groups. The cells received treatment with free Nile Red, Nile Red-loaded PEG-PLGA micelles (non-targeted), and Nile Red-loaded FA-PEG-PLGA micelles (targeted), with untreated cells as the control group.

After a 24-hour incubation period, the cells were fixed and stained with DAPI and Concanavalin A Alexa Fluor™ 488 for visualising nuclei and cell membranes, respectively.

The analysis indicated negligible fluorescence in untreated control cells, confirming expectations. Cells treated with free Nile Red exhibited weak and diffuse intracellular fluorescence, demonstrating limited passive uptake. In contrast, cells that received Nile Red-loaded PEG-PLGA micelles showed enhanced fluorescence intensity, suggesting improved internalisation through micelle-mediated delivery. Notably, the FA-PEG-PLGA group exhibited the most significant Nile Red fluorescence, which indicates enhanced cellular uptake likely attributed to folate receptor-mediated endocytosis.

These results highlight the targeting effectiveness of FA-modified micelles in folate receptor-positive ovarian cancer cells and affirm the system's potential for efficient intracellular delivery of hydrophobic compounds.

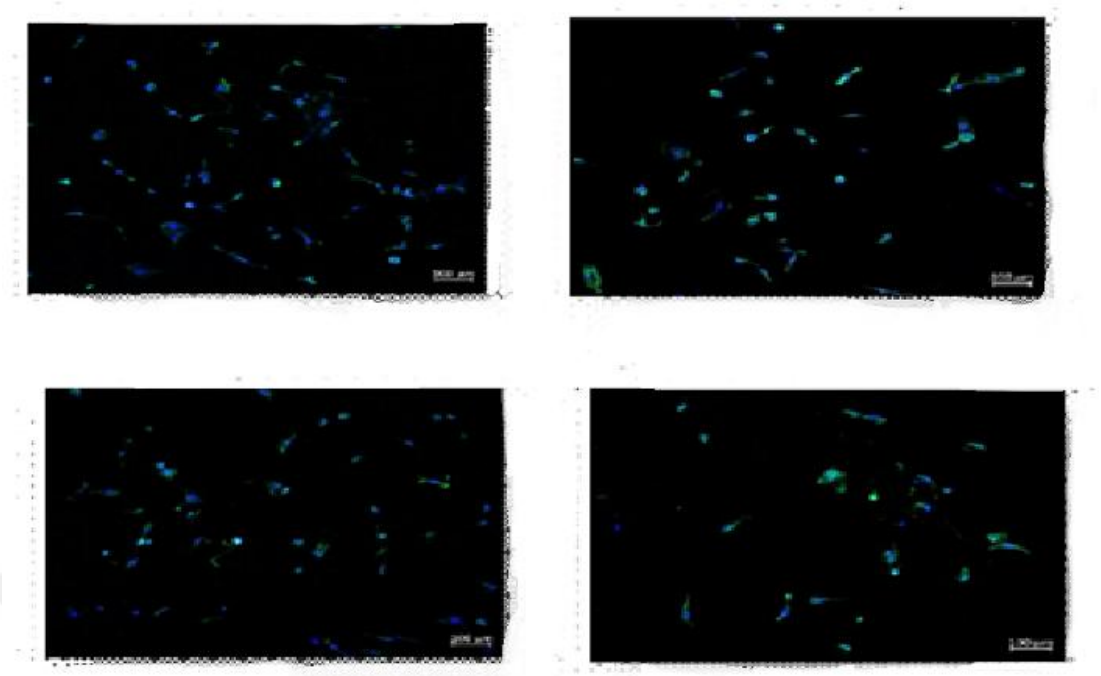

Figure 4.26. 0 hour Cell Imaging with DAPI and Alexa Fluor. Since it was 0th hour no Nile Red was observed.

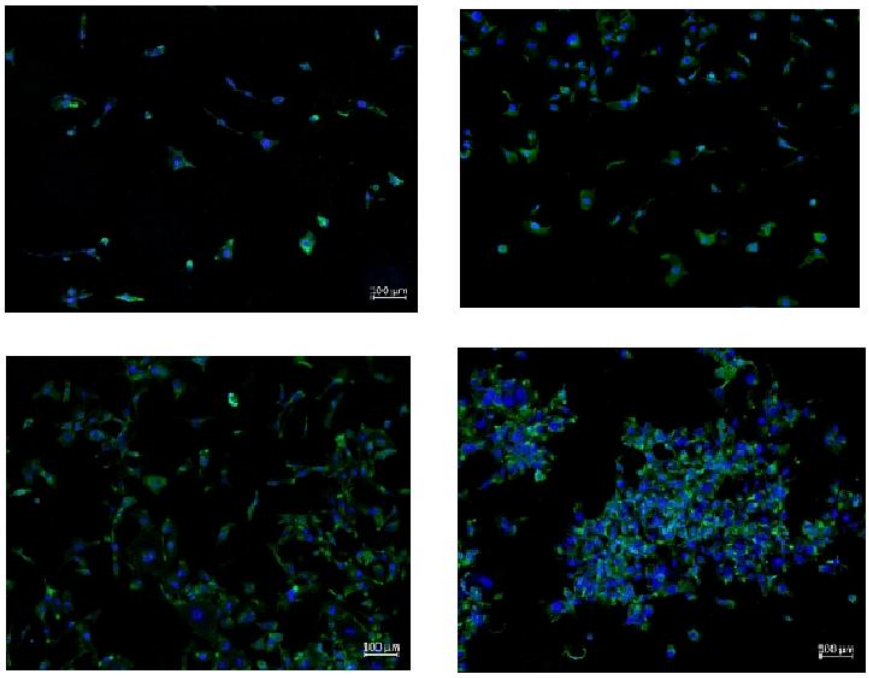

Figure 4.27. 2-hour Cell Imaging with DAPI and Alexa Fluor. Since it was 2nd hour no Nile Red was observed.

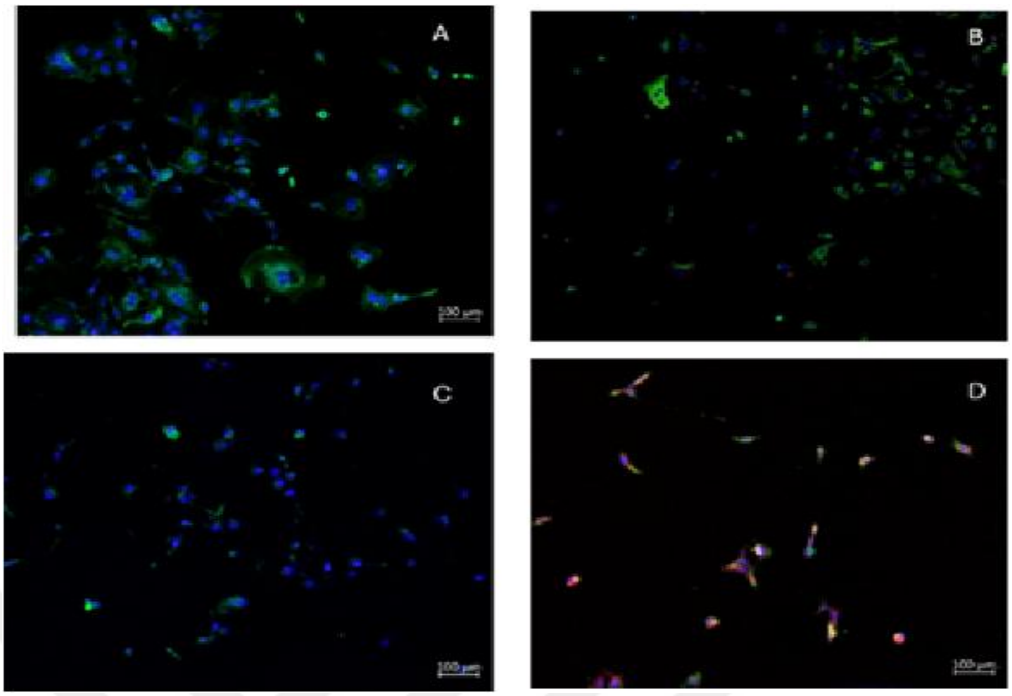

Figure 4.28. 4-hour Cell Imaging with DAPI and Alexa Fluor. Since it was the 4th hour Nile Red was observed in only on (D) targeted approach

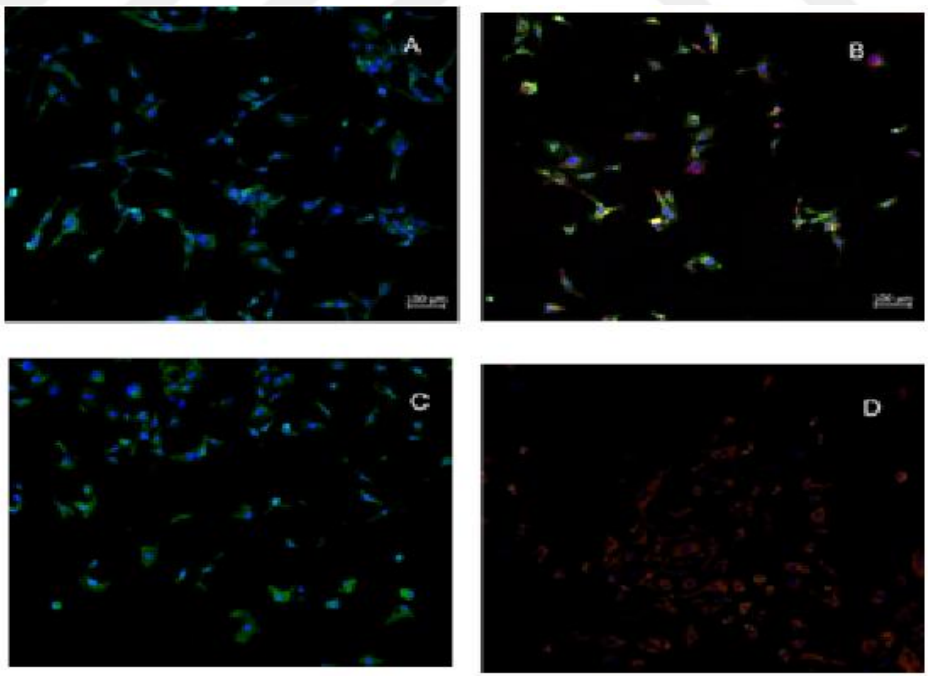

Figure 4.29. 6-hour Cell Imaging with DAPI and Alexa Fluor. Since it was the 6th hour Nile Red was observed in (A) direct and (D) targeted approaches

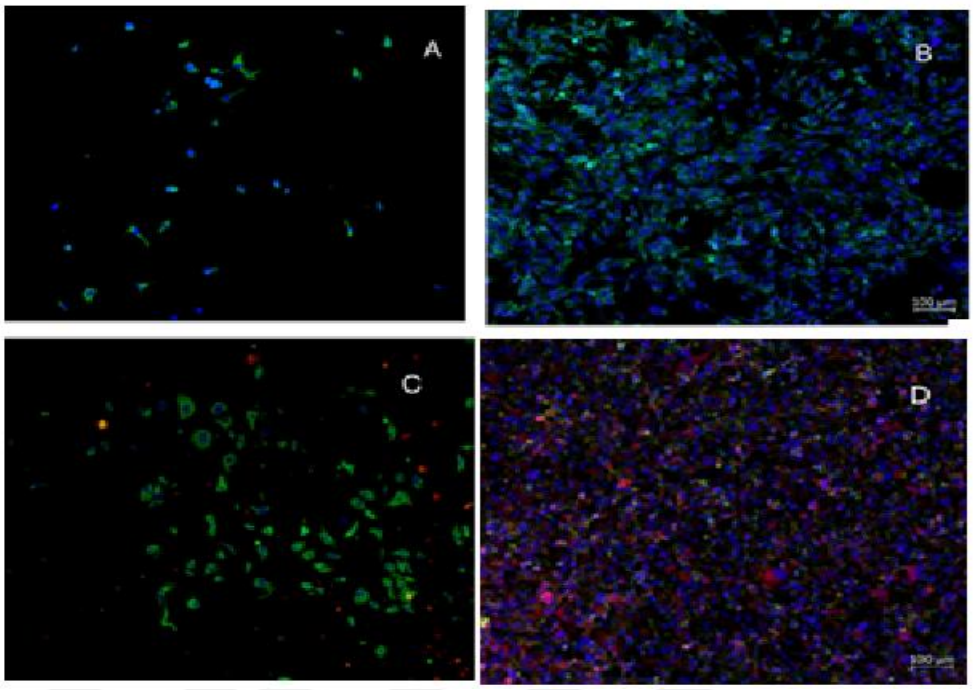

Figure 4.30. 24-hour Cell Imaging with DAPI and Alexa Fluor. Since it was the 24th hour Nile Red was observed in (C) non-targeted and (D) targeted approaches

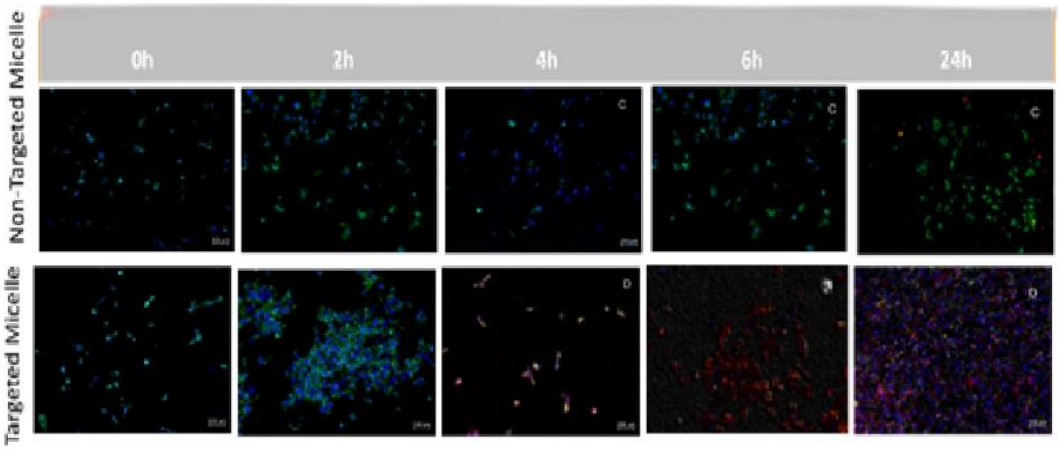

Figure 4.31. Time-dependent cellular imaging over 24 hours using DAPI and Alexa Fluor staining. Nile Red fluorescence became evident at the 24-hour mark in both (C) non-targeted and (D) targeted formulations.

5. DISCUSSION

The development of targeted drug delivery systems is a cornerstone in improving the therapeutic index of PARP inhibitors like 3-aminobenzamide (3-AB). In this study, folate-targeted PEG–PLGA micelles were successfully developed and characterized to enhance the delivery of 3-AB to SKOV-3 ovarian cancer cells. The characterization studies confirmed the formation of stable micelles with suitable particle sizes for tumor accumulation.

The biocompatibility of the polymeric carrier is a fundamental requirement for clinical translation. Our results from the CCK-8 assay (Figure 4.20) demonstrated that the empty PLGA–PEG micelles exhibit high biocompatibility. Even at the highest tested concentration of 100 µg/mL, cell viability remained at 75.95%. This finding is crucial as it confirms that the observed anti-cancer effects in drug-loaded formulations are exclusively due to the therapeutic action of 3-AB and its targeted delivery, rather than any intrinsic toxicity of the polymer matrix itself. This safety profile is consistent with other PEG-PLGA based delivery systems reported in literature.

A critical aspect of the formulation was the optimization of the targeting ligand ratio. Based on preliminary studies evaluating different weight ratios (2%, 4%, and 10% w/w), the 4% (w/w) FA-PEG-PLGA functionalization was identified as the optimal concentration for achieving effective receptor-mediated endocytosis. This specific ratio provided the best balance between targeting efficiency and physical stability of the micelles during the preparation process. The enhanced cellular internalization observed in Nile Red studies further reinforces the advantage of using a 4% folate-targeted approach for SKOV-3 cells, which are known to overexpress folate receptors.

Regarding drug loading, the encapsulation efficiency (EE%) showed a clear dependency on the initial drug-to-polymer ratio. The highest EE% values were achieved at a 5% loading ratio (94.4% for non-targeted and 86.1% for targeted micelles). The observed decrease in efficiency at higher drug feeds (up to 20%) suggests that the hydrophobic core of the PEG-PLGA micelles reached a saturation point. These findings are important for determining the final dosage and the frequency of administration in potential in vivo applications.

The in vitro cytotoxicity results of 3-AB loaded micelles indicated a dose-dependent decrease in cell viability across all formulations. The targeted micelles showed a more pronounced inhibitory effect compared to free drug and non-targeted counterparts, particularly at higher concentrations. This underscores the effectiveness of the folate-mediated uptake mechanism. Overall, the integration of 4% FA-targeting with highly biocompatible PEG-PLGA micelles presents a promising strategy for overcoming the pharmacokinetic limitations of PARP inhibitors in ovarian cancer treatment, paving the way for further research.

6. CONCLUSION

In this study, a novel drug delivery system based on folic acid (FA)-functionalized PEG–PLGA micelles was developed for the encapsulation and targeted delivery of 3-aminobenzamide (3-AB). The primary goal was to enhance the therapeutic performance and cellular uptake of 3-AB, which has limited clinical utility due to its poor bioavailability and rapid metabolism. The micelles were synthesized using a solvent evaporation method and characterized extensively. The results confirmed the successful formation of nanoscale, colloidally stable, and uniform micelles suitable for biological applications.

Biological assessments using the SKOV-3 ovarian cancer cell line demonstrated that the developed formulations significantly outperformed free 3-AB. A key finding of this research was the identification of the **4% (w/w) FA-PEG-PLGA** ratio as the optimal concentration for achieving effective targeting. Furthermore, the empty micellar carrier demonstrated high biocompatibility, with cell viability remaining at **75.95%** even at the highest concentration of 100 µg/mL. This underscores that the observed cytotoxic effects in the targeted groups are specifically due to the ligand-receptor mediated endocytosis.

The observed results clearly underscore the synergistic effect of both PEGylation and **4% FA-targeting** in achieving improved therapeutic performance. Although the outcomes of this research are promising, certain limitations remain, such as the need for in vivo validation to investigate the biodistribution and pharmacokinetics of these FA-PEG–PLGA micelles. The characterization and in vitro data provide a strong

foundation for these future studies, suggesting that the system can be adapted for other hydrophobic PARP inhibitors.

In conclusion, the findings presented in this thesis support the notion that folate receptor-targeted, PEGylated polymeric micelles provide a promising nanocarrier platform for the efficient and selective delivery of 3-AB. This approach offers significant advantages in overcoming conventional drug limitations and opens new avenues for personalized cancer therapies. The integration of 4% targeting with a highly safe carrier (75.95% viability) ensures both efficacy and biocompatibility, making this formulation a strong candidate for further pharmaceutical development.

7. REFERENCES

1. Zhang L, Gu FX, Chan JM, Wang AZ, Langer RS, Farokhzad OC. Nanoparticles in medicine: therapeutic applications and developments. Clin Pharmacol Ther. 2008;83(5):761–9. Available from: https://doi.org/10.1038/clpt.2008.67

2. Torchilin VP. Multifunctional nanocarriers. Adv Drug Deliv Rev. 2006;58(14):1532–55. Available from: https://doi.org/10.1016/j.addr.2006.09.009

3. Wang Y, Zhang L, Wang Q, Zhang D. Folate-targeted biodegradable PEG–PLGA micelles for drug delivery: synthesis, characterization, and targeting ability. Int J Pharm. 2013;450(1-2):248–57. Available from: https://doi.org/10.1016/j.ijpharm.2013.01.027

4. Mu L, Feng SS. A novel controlled release formulation for the anticancer drug paclitaxel (Taxol®): PLGA nanoparticles containing vitamin E TPGS. J Control Release. 2003;86(1):33–48. Available from: https://doi.org/10.1016/S0168-3659(02)00310-6

5. Allen TM, Cullis PR. Drug delivery systems: entering the mainstream. Science. 2004;303(5665):1818–22. Available from: https://doi.org/10.1126/science.1095833

6. Bertrand N, Wu J, Xu X, Kamaly N, Farokhzad OC. Cancer nanotechnology: the impact of passive and active targeting in the era of modern cancer biology. Adv Drug Deliv Rev. 2014;66:2–25. Available from: https://doi.org/10.1016/j.addr.2013.11.009

7. Jain RK, Stylianopoulos T. Delivering nanomedicine to solid tumors. Nat Rev Clin Oncol. 2010;7(11):653–64. Available from: https://doi.org/10.1038/nrclinonc.2010.139

8. Liu Y, et al. Binding and orientation of antibodies immobilized onto gold nanoparticles. Langmuir. 2019;35(6):1864–72. Available from: https://doi.org/10.1021/acs.langmuir.8b03510

9. Chatterjee N, Eom HJ, Choi J. Effect of silver nanoparticles on oxidative stress and DNA damage in human cells. Cancer Lett. 2014;312(2):167–75. Available from: https://doi.org/10.1016/j.canlet.2011.08.011

10. Banerjee A, Qi J, Gogoi R, Wong J, Mitra AK. Role of nanoparticle size, shape and surface chemistry in oral drug delivery. J Control Release. 2011;238:176–85. Available from: https://doi.org/10.1016/j.jconrel.2016.07.051

11. Maeda H, Wu J, Sawa T, Matsumura Y, Hori K. Tumor vascular permeability and the EPR effect in macromolecular therapeutics: a review. J Control Release. 2000;65(1–2):271–84.

12. Liu D, Auguste DT. Cancer targeted therapeutics: from molecules to drug delivery vehicles. J Control Release. 2015;219:632–43.

13. Wang M, Thanou M. Targeting nanoparticles to cancer. Pharmacol Res. 2010;62(2):90–9.

14. Fang J, Nakamura H, Maeda H. The EPR effect: unique features of tumor blood vessels for drug delivery, factors involved, and limitations and augmentation of the effect. Adv Drug Deliv Rev. 2011;63(3):136–51.

15. Owens DE, Peppas NA. Opsonization, biodistribution, and pharmacokinetics of polymeric nanoparticles. Int J Pharm. 2006;307(1):93–102.

16. Reddy LH, Couvreur P. Nanotechnology for therapy and imaging of liver diseases. J Hepatol. 2011;55(6):1461–6.

17. Shi J, Kantoff PW, Wooster R, Farokhzad OC. Cancer nanomedicine: progress, challenges and opportunities. Nat Rev Cancer. 2017;17(1):20–37.

18. Tibbitt MW, Dahlman JE, Langer R. Emerging frontiers in drug delivery. Nat Rev Mater. 2016;1(7):1–15.

19. Min Y, Caster JM, Eblan MJ, Wang AZ. Clinical translation of nanomedicine. Chem Rev. 2015;115(19):11147–90.

20. Hafner A, Lovrić J, Lakoš GP, Pepić I. Nanotherapeutics in cancer: challenges and future perspectives. Acta Pharm. 2014;64(3):371–87.

21. Torchilin VP. Multifunctional, stimuli-sensitive nanoparticulate systems for drug delivery. Nat Rev Drug Discov. 2011;13(11):813–27.

22. Li W, Szoka FC. Lipid-based nanoparticles for nucleic acid delivery. Pharmacol Res. 2007;24(3):438–49.

23. Natarajan A, Xie Y, Baik FM. Targeted nanomedicine for cancer therapy. Theranostics. 2012;2(3):294–312.

24. Ma X, Zhao Y. Biomedical applications of supramolecular systems based on host–guest interactions. Chem Rev. 2015;115(15):7794–839.

25. He Q, Shi J. MSN anti-cancer nanomedicines: chemotherapy enhancement, overcoming of drug resistance, and metastasis inhibition. Adv Mater. 2011;23(38):H57–77.

26. Nasongkla N, et al. cRGD-functionalized polymer micelles for targeted doxorubicin delivery. Bioconjug Chem. 2004;15(4):734–40.

27. Zhou J, Wang CH. pH-sensitive polymeric nanoparticles for drug delivery. Curr Pharm Des. 2012;18(25):3517–24.

28. Adams ML, Lavasanifar A, Kwon GS. Amphiphilic block copolymers for drug delivery. J Pharm Sci. 2003;92(7):1343–55.

29. Parveen S, Misra R, Sahoo SK. Nanoparticles: a boon to drug delivery, therapeutics, diagnostics and imaging. Nanomedicine. 2012;8(2):147–66.

30. Jain KK. The role of nanobiotechnology in drug discovery. Drug Discov Today. 2005;10(21):1435–42.

31. Peer D, Karp JM, Hong S, Farokhzad OC, Margalit R, Langer R. Nanocarriers as an emerging platform for cancer therapy. Nat Nanotechnol. 2007;2(12):751–60. Available from: https://doi.org/10.1038/nnano.2007.387

32. Cho K, Wang X, Nie S, Chen ZG, Shin DM. Therapeutic nanoparticles for drug delivery in cancer. Clin Cancer Res. 2008;14(5):1310–6.

33. Wicki A, Witzigmann D, Balasubramanian V, Huwyler J. Nanomedicine in cancer therapy: challenges, opportunities, and clinical applications. J Control Release. 2015;200:138–57.

34. Kim TH, Jiang HH, Youn YS, Lee S. PEGylated poly(lactic-co-glycolic acid) nanoparticles for enhanced delivery of hydrophobic anticancer drugs. J Biomed Nanotechnol. 2015;11(11):2032–42.

35. Sahoo SK, Labhasetwar V. Nanotech approaches to delivery and imaging drug. Drug Discov Today. 2003;8(24):1112–20.

36. Hrkach J, et al. Preclinical development and clinical translation of a PSMA-targeted docetaxel nanoparticle with a differentiated pharmacological profile. Sci Transl Med. 2012;4(128):128ra39.

37. Yin H, Kanasty RL. Non-viral vectors for gene-based therapy. Nat Rev Genet. 2014;15(8):541–55.

38. Nel AE, et al. Understanding biophysicochemical interactions at the nano–bio interface. Nat Mater. 2009;8(7):543–57.

39. Duncan R, Vicent MJ. Polymer therapeutics—prospects for 21st century: the end of the beginning. Adv Drug Deliv Rev. 2013;65(1):60–70.

40. Klibanov AL. Microbubble contrast agents: targeted ultrasound imaging and ultrasound-assisted drug-delivery applications. Invest Radiol. 2005;41(3):354–62.

41. Wang AZ, Gu F, Zhang L, Chan JM, Radovic-Moreno AF, Shaikh MR, Farokhzad OC. Biofunctionalized targeted nanoparticles for therapeutic applications. Expert Opin Biol Ther. 2008;8(8):1063–70.

42. Allen TM, Cullis PR. Liposomal drug delivery systems: from concept to clinical applications. Adv Drug Deliv Rev. 2013;65(1):36–48.

43. Blanco E, Shen H, Ferrari M. Principles of nanoparticle design for overcoming biological barriers to drug delivery. Nat Biotechnol. 2015;33(9):941–51.

44. Kamaly N, Yameen B, Wu J, Farokhzad OC. Degradable controlled-release polymers and polymeric nanoparticles: mechanisms of controlling drug release. Chem Rev. 2016;116(4):2602–63.

45. Suh J, Dawson M, Hanes J. Real-time multiple-particle tracking: applications to drug and gene delivery. Adv Drug Deliv Rev. 2005;57(1):63–78.

46. Nirmala MJ, Nagarajan R. PEGylated nanocarriers for tumor targeted delivery: A review. Adv Drug Deliv Rev. 2021;179:113983.

47. Ramasamy T, et al. PEGylated lipid–polymer hybrid nanoparticles: A promising platform for improved stability and bioavailability of anticancer drugs. Int J Pharm. 2014;474(1–2):20–31.

48. Barabadi H, et al. Green synthesis of metallic nanoparticles using plants. J Nanostruct Chem. 2019;9:1–15.

49. Novoselov KS, et al. Electric field effect in atomically thin carbon films. Science. 2004;306(5696):666–9.

50. Bhushan B. Springer Handbook of Nanotechnology. Berlin: Springer; 2017.

51. Murray CB, et al. Synthesis and characterization of nearly monodisperse CdE (E = S, Se, Te) semiconductor nanocrystallites. J Am Chem Soc. 2000;122(7):1237–8.

52. Ma PX. Biomimetic materials for tissue engineering. Adv Drug Deliv Rev. 2008;60(2):184–98.

53. Wang Y, et al. Classification and characterization of nanoparticles in nanotechnology. Environ Toxicol Chem. 2013;32(4):738–46.

54. Barui A, Banerjee R. Potential of folate receptor-targeted liposomes in drug delivery. Ther Deliv. 2012;3(8):995–1005.

55. Haes AJ, Van Duyne RP. Localized surface plasmon resonance sensors. Chem Rev. 2019;119(2):1235–60.

56. Zhang L, et al. Enhance photocatalysis of TiO_2 and ZnO ceramics by addition of functional layers. J Catal. 2017;348:120–33.

57. Li X, Zhao Y. Review of recent developments in ZnS photocatalysts for water splitting. Chem Eng J. 2023;450:138–52.

58. Serpico L, et al. Lipid nanoparticles-based RNA therapies for breast cancer treatment. Drug Deliv Transl Res. 2024;14:2823–44.

59. Smith JT, et al. Polymeric nanoparticles engineered for optimal drug delivery and gene therapy. ACS Appl Nano Mater. 2024;7(6):3100–20.

60. Alexis F, Pridgen E, Molnar LK, Farokhzad OC. Factors affecting the clearance and biodistribution of polymeric nanoparticles. Mol Pharm. 2008;5(4):505–15. Available from: https://doi.org/10.1021/mp800051m

61. Kumari A, Yadav SK, Yadav SC. Biodegradable polymeric nanoparticles based drug delivery systems. Colloids Surf B Biointerfaces. 2010;75(1):1–18. Available from: https://doi.org/10.1016/j.colsurfb.2009.09.001

62. Danhier F, Ansorena E, Silva JM, Coco R, Le Breton A, Préat V. PLGA-based nanoparticles: An overview of biomedical applications. J Control Release. 2012;161(2):505–22. Available from: https://doi.org/10.1016/j.jconrel.2012.01.043

63. Blanco E, Shen H, Ferrari M. Principles of nanoparticle design for overcoming biological barriers to drug delivery. Nat Biotechnol. 2015;33(9):941–51. Available from: https://doi.org/10.1038/nbt.3330

64. Sahana DK, Rekha PD, Kumar MNV. Polymeric nanoparticles and their applications in drug delivery: a review. Int J Drug Deliv. 2010;2(1):20–32. Available from: https://doi.org/10.5138/ijdd.2010.0975.0215.02032

65. Zhang RX, Wong HL, Xue HY, Eoh JY, Wu XY. Nanomedicine-based delivery of RNAi therapeutics: progress and challenges. Pharm Res. 2016;33(10):2131–55.

66. Farokhzad OC, Langer R. Impact of nanotechnology on drug delivery. ACS Nano. 2009;3(1):16–20. Available from: https://doi.org/10.1021/nn900002m

67. Makadia HK, Siegel SJ. Poly lactic-co-glycolic acid (PLGA) as biodegradable controlled drug delivery carrier. Polymers (Basel). 2011;3(3):1377–97. Available from: https://doi.org/10.3390/polym3031377

68. Makadia HK, Siegel SJ. Poly lactic-co-glycolic acid (PLGA) as biodegradable controlled drug delivery carrier. Polymers (Basel). 2011;3(3):1377–97. Available from: https://doi.org/10.3390/polym3031377

69. Singh R, Lillard JW. Nanoparticle-based targeted drug delivery. Exp Mol Pathol. 2009;86(3):215–23. Available from: https://doi.org/10.1016/j.yexmp.2009.01.004

70. Kwon GS, Okano T. Polymeric micelles as new drug carriers. Adv Drug Deliv Rev. 1996;21(2):107–16. Available from: https://doi.org/10.1016/0169-409X(95)00044-M

71. Duncan R. The dawning era of polymer therapeutics. Nat Rev Drug Discov. 2003;2(5):347–60. Available from: https://doi.org/10.1038/nrd1088

72. Torchilin VP. Micellar nanocarriers: pharmaceutical perspectives. Pharm Res. 2007;24(1):1–16. Available from: https://doi.org/10.1007/s11095-006-9121-0

73. Park K. Controlled drug delivery systems: past forward and future back. J Control Release. 2014;190:3–8. Available from: https://doi.org/10.1016/j.jconrel.2014.03.054

74. Danhier F, Ansorena E, Silva JM, Coco R, Le Breton A, Préat V. PLGA-based nanoparticles: An overview of biomedical applications. J Control Release. 2012;161(2):505–22. Available from: https://doi.org/10.1016/j.jconrel.2012.01.043

75. Gabizon A, Shmeeda H, Barenholz Y. Pharmacokinetics of pegylated liposomal Doxorubicin: review of animal and human studies. Clin Pharmacokinet. 2003;42(5):419–36.

76. Jokerst JV, Lobovkina T, Zare RN, Gambhir SS. Nanoparticle PEGylation for imaging and therapy. Nanomedicine. 2011;6(4):715–28. Available from: https://doi.org/10.2217/nnm.11.19

77. Park K. Controlled drug delivery systems: past forward and future back. J Control Release. 2014;190:3–8. Available from: https://doi.org/10.1016/j.jconrel.2014.03.054

78. Makadia HK, Siegel SJ. Poly lactic-co-glycolic acid (PLGA) as biodegradable controlled drug delivery carrier. Polymers (Basel). 2011;3(3):1377–97. Available from: https://doi.org/10.3390/polym3031377

79. Gabizon A, Shmeeda H, Barenholz Y. Pharmacokinetics of pegylated liposomal Doxorubicin: review of animal and human studies. Clin Pharmacokinet. 2003;42(5):419–36.

80. Anderson JM, Shive MS. Biodegradation and biocompatibility of PLA and PLGA microspheres. Adv Drug Deliv Rev. 1997;28(1):5–24. Available from: https://doi.org/10.1016/S0169-409X(97)00048-3

81. Kamaly N, Yameen B, Wu J, Farokhzad OC. Degradable controlled-release polymers and polymeric nanoparticles: mechanisms of controlling drug release. Chem Rev. 2016;116(4):2602–63.

82. Danhier F, Ansorena E, Silva JM, Coco R, Le Breton A, Préat V. PLGA-based nanoparticles: An overview of biomedical applications. J Control Release. 2012;161(2):505–22.

83. Owens DE, Peppas NA. Opsonization, biodistribution, and pharmacokinetics of polymeric nanoparticles. Int J Pharm. 2006;307(1):93–102.

84. Suk JS, Xu Q, Kim N, Hanes J, Ensign LM. PEGylation as a strategy for improving nanoparticle-based drug and gene delivery. Adv Drug Deliv Rev. 2016;99:28–51.

85. Veronese FM, Pasut G. PEGylation, successful approach to drug delivery. Drug Discov Today. 2005;10(21):1451–8.

86. Knop K, Hoogenboom R, Fischer D, Schubert US. Poly(ethylene glycol) in drug delivery: pros and cons as well as potential alternatives. Angew Chem Int Ed Engl. 2010;49(36):6288–308.

87. Zhang P, Sun F, Liu S, Jiang S. Anti-PEG antibodies in the clinic: current issues and beyond PEGylation. J Control Release. 2016;244:184–93.

88. Zhang L, Gu FX, Chan JM, Wang AZ, Langer RS, Farokhzad OC. Nanoparticles in medicine: therapeutic applications and developments. Clin Pharmacol Ther. 2008;83(5):761–9.

89. Sperling RA, Rivera Gil P, Zhang F, Zanella M, Parak WJ. Biological applications of gold nanoparticles. Chem Soc Rev. 2008;37(9):1896–906.

90. Kuo WS, Chang CN. Surface functionalization of nanoparticles for drug delivery. J Mater Chem. 2011;21(19):7255–63.

91. Boisselier E, Astruc D. Gold nanoparticles in nanomedicine: preparations, imaging, diagnostics, therapies and toxicity. Chem Soc Rev. 2009;38(6):1759–82.

92. Tasis D, Tagmatarchis N, Bianco A, Prato M. Chemistry of carbon nanotubes. Chem Rev. 2006;106(3):1105–1136.

93. Allen TM, Cullis PR. Drug delivery systems: entering the mainstream. Science. 2004;303(5665):1818–22.

94. Hermanson GT. Bioconjugate Techniques. 3rd ed. San Diego: Academic Press; 2013.

95. Prime KL, Whitesides GM. Self-assembled organic monolayers: model systems for studying adsorption of proteins at surfaces. Science. 1991;252(5009):1164–7. Available from: https://doi.org/10.1126/science.252.5009.1164

96. Sperling RA, Parak WJ. Surface modification, functionalization and bioconjugation of colloidal inorganic nanoparticles. Philos Trans A Math Phys Eng Sci. 2010;368(1915):1333–73. Available from: https://doi.org/10.1098/rsta.2009.0273

97. Wang J, Liu G, Jan MR. Ultrasensitive electrical biosensing of proteins and DNA: carbon-nanotube derived amplification of the recognition and transduction events. J Am Chem Soc. 2004;126(10):3010–11. Available from: https://doi.org/10.1021/ja031873l

98. Knop K, Hoogenboom R, Fischer D, Schubert US. Poly(ethylene glycol) in drug delivery: pros and cons as well as potential alternatives. Angew Chem Int Ed Engl. 2010;49(36):6288–308.

99. Veronese FM, Mero A. The impact of PEGylation on biological therapies. BioDrugs. 2008;22(5):315–29.

100. Fee CJ, Van Alstine JM. Prediction of the viscosity Diameter and the size exclusion chromate Figurey behavior of PEGylated proteins. Bioconjug Chem. 2004;15(6):1304–13.

101. Yang Q, Lai SK. Anti-PEG immunity: emergence, characteristics, and unaddressed questions. Wiley Interdiscip Rev Nanomed Nanobiotechnol. 2015;7(5):655–77. Available from: https://doi.org/10.1002/wnan.1339

102. Suk JS, Xu Q, Kim N, Hanes J, Ensign LM. PEGylation as a strategy for improving nanoparticle-based drug and gene delivery. Adv Drug Deliv Rev. 2016;99(Pt A):28–51. Available from: https://doi.org/10.1016/j.addr.2015.09.012

103. Lu Y, Low PS. Folate-mediated delivery of macromolecular anticancer therapeutic agents. Adv Drug Deliv Rev. 2012;64(11):342–52.

104. Torre LA, Trabert B, DeSantis CE, Miller KD, Samimi G, Runowicz CD, et al. Ovarian cancer statistics, 2018. CA Cancer J Clin. 2018;68(4):284–96. Available from: https://doi.org/10.3322/caac.21456

105. Ledermann JA, Raja FA, Fotopoulou C, Gonzalez-Martin A, Colombo N, Sessa C. Newly diagnosed and relapsed epithelial ovarian carcinoma: ESMO Clinical Practice Guidelines. Ann Oncol. 2013;24 Suppl 6:vi24–32. Available from: https://doi.org/10.1093/annonc/mdt333

106. Lord CJ, Ashworth A. PARP inhibitors: synthetic lethality in the clinic. Science. 2017;355(6330):1152–8. Available from: https://doi.org/10.1126/science.aam7344

107. Patra JK, Das G, Fraceto LF, Campos EVR, Rodriguez-Torres MDP, Acosta-Torres LS, et al. Nano based drug delivery systems: recent developments and future prospects. J Nanobiotechnology. 2018;16(1):71. Available from: https://doi.org/10.1186/s12951-018-0392-8

108. Mehmood T, Ahmed N, Sarwar HS, Hussain SZ, Shahnaz G, Hussain A, et al. Co-delivery of docetaxel and gemcitabine via folate-decorated PEG–PLGA nanoparticles for enhanced ovarian cancer therapy. Drug Dev Ind Pharm. 2022;48(1):64–72. Available from: https://doi.org/10.1080/03639045.2021.2003499

109. Ciccia A, Elledge SJ. The DNA damage response: making it safe to play with knives. Mol Cell. 2010;40(2):179–204. Available from: https://doi.org/10.1016/j.molcel.2010.09.019

110. Lord CJ, Ashworth A. PARP inhibitors: synthetic lethality in the clinic. Science. 2017;355(6330):1152–8.
111. Anwar S, Siddiqui FA. Nanoparticle-mediated drug delivery of PARP inhibitors for cancer therapy: recent advances and challenges. Int J Pharm. 2021;597:120329.
112. Chatterjee N, Walker GC. Mechanisms of DNA damage, repair, and mutagenesis. Environ Mol Mutagen. 2017;58(5):235–63.
113. Faraoni I, Graziani G, Damia G. Pharmacokinetics and pharmacodynamics of PARP inhibitors. Cancer Treat Rev. 2015;41(10):896–904.
114. Reles A, et al. Correlation of p53 mutations with resistance to platinum-based chemotherapy and shortened survival in ovarian cancer. Clin Cancer Res. 2001;7(12):2984–97.
115. Ekmekcioglu A, Gok O, Oz-Arslan D, Erdal MS, Yagan Uzuner Y, Muftuoglu M. Mitochondria-targeted liposomes for drug delivery to tumor mitochondria. Pharmaceutics. 2024;16(7):950. Available from: https://doi.org/10.3390/pharmaceutics16070950
116. Zhao Y, et al. Targeted nanocarrier delivery of chemotherapeutics to folate receptor-positive ovarian cancer. Biomaterials. 2015;65:34–46.
117. Fouladiha H, et al. Folic acid-conjugated nanoparticles for targeted cancer therapy. Drug Discov Today. 2020;25(7):1268–76.
118. Patra JK, et al. Application of nanotechnology in diagnosis and treatment of ovarian cancer. Biomed Pharmacother. 2022;146:112647.
119. Mehmood T, et al. Folic acid-functionalized nanocarriers for enhanced delivery of chemotherapeutics in ovarian cancer. J Drug Deliv Sci Technol. 2022;67:102972.
120. Kesharwani P, et al. Nanocarriers for cancer-targeted drug delivery. J Control Release. 2015;220:138–49.
121. Maeda H, et al. The EPR effect: unique features of tumor blood vessels for drug delivery, factors involved, and limitations and augmentation of the effect. Adv Drug Deliv Rev. 2013;63(3):136–51.

8. CURRICULUM VITAE